Supplementary Information

Divergent Evolution of Fungal P450 Monooxygenase Unlocks Simultaneous Access to C12β and C15α Oxyfunctionalization of Steroids

Wang, Wang, Peng et al.

Materials and methods 1

Commercial Materials 1

Strains, plasmids and media 1

NMR and HRMS Characterization of the Products 2

NMR and HR-EMIMS data 3

Supplementary Tables 6

Supplementary Table 1. Diverse electronic states in the QM model of CYP68J5_fg (Cpd I) with substrate (**1**) bound at pose 12. 6

Supplementary Table 2. Diverse electronic states in the QM model of CYP68J5_fg (Cpd I) with substrate (**1**) bound at pose 15. 6

Supplementary Figures 7

Supplementary Figure 1. MD simulations of W12M5 in pose 12 in the reaction with **1**. 7

Supplementary Figure 2. MD simulations of W15M4 in pose 15 in the reaction with **1**. 8

Supplementary Figure 3. Potential energy profiles for the CYP68J5_fg-catalyzed C(12,15)-hydroxylation of **1**. 9

Supplementary Figure 4. QM-optimized transition-state structures for C(12,15)-H abstraction in **1**. 9

Supplementary Figure 5. Plot of the distances of H-bonds for three independent MD simulations with **1** bound in CYP68J5_fg mutants, W12M5 and W15M4. 10

Supplementary Figure 6. MD simulations of CYP68J5_fg and its variants in the non-productive position with **1**. 12

Supplementary Figure 7. Representative Snapshots from MD Simulations of the W12M5-**1** Complex. 12

Supplementary Figure 8. The selectivity and activity results of different mutants towards various substrates were screened using 96-well plates. 13

Supplementary Figure 9. Bioconversion of 1 mM AD by AYR1 from *P. pastoris* in *E. coli* [2]. 13

Supplementary Figure 10. MD simulations of CYP68J5_fg variants with steroids. 14

Supplementary Figure 11. Conversion of **1** by the CYP68J5_fg mutants in *P. pastoris.* 15

Supplementary Figure 12. Relative activity of GS115-W12M5 after 24 h reaction with simultaneous addition of varying concentrations of 1a and 5 mM substrate **1**. 16

Supplementary Figure 13. Conversion of **1** by the GS115-W15M4 in *P. pastoris*. 16

Supplementary Figures for NMR 17

Supplementary Figures for HR-EMIMS 38

Supplementary References 40

Materials and methods

Commercial Materials

Primer STAR Max DNA Polymerase was purchased from Takara (Shanghai, China). Restriction enzyme *Dpn*I and *Pme*I were purchased from NEB (Beijing, China). KOD Neo DNA polymerase was purchased from TOYOBO (Shanghai, China). DNA Marker and TS-GelRed Nucleic acid dye were purchased from TSINGKE (Beijing, China). Plasmid Miniprep Purification Kit and DNA Clean/Extraction Kit were ordered from TransGen Biotech (Beijing, China) and Omega (USA), respectively. TIANprep Yeast Plasmid DNA Kit was ordered from Tiangen Biotech (Beijing, China). Oligonucleotide primers syntheses and DNA sequencing were conducted by Sangon (Shanghai, China). Ampicillin antibiotic was bought from Sangon (Shanghai, China) and Zeocin® (solution) was bought from InvivoGen. Steroid substrates and (2-Hydroxypropyl)-*β*-cyclodextrin were purchased from Aladdin (Shanghai, China). Tryptone and yeast extract were purchased from OXOID (Shanghai, China). DMF and general chemicals were purchased from HUSHI (Shanghai, China). Other chemicals were of chemical purity and commercially available. Millipore ultrapure water was used in all experiments.

Strains, plasmids and media

The gene encoding CYP68J5_fg in a pYES2 vector was codon-optimized for expression in *Saccharomyces cerevisiae* (*S. cerevisiae*) strain INVSc1 [1]. The *Pichia pastoris* (*P. pastoris*) strains were derived from HIS4 auxotrophic *P. pastoris* GS115, and the gene encoding CYP68J5_fg in a pPICZ vector was codon-optimized for expression in GS115. *E. coli* DH5*α* was used as hosts for gene cloning. The Luria-Bertani (LB) medium (5 g/L yeast extract, 10 g/L tryptone, 10 g/L NaCl) was used for cultivating *E. coli* DH5α, which was incubated at 37 °C with shaking at 220 rpm, and supplemented with 100 μg/mL ampicillin or 25 μg/mL zeocin when required. Uracil dropout minimal medium (6.7 g/L of yeast nitrogen base; 0.1 g/L of adenine, arginine, cysteine, leucine, lysine, threonine, and tryptophan, 0.05 g/L of aspartic acid, histidine, isoleucine, methionine, phenylalanine, proline, serine, tyrosine, valine, and either 2% (w/v) glucose or 4% (w/v) galactose as the carbon source) was used to culture *S.cerevisiae*. YPD solid medium (20 g/L glucose, 20 g/L tryptone and 10 g/L yeast extract) with 100 μg/mL

zeocin was used to screen *P. pastoris* transformants. Recombinant *P. pastoris* strains were cultivated in BMGY medium (10 g/L yeast extract, 20 g/L tryptone, 13.4 g/L YNB, 100 mM potassium phosphate buffer pH 6.0 and 10 g/L glycerol) at 30℃ and induced in BMMY medium (10 g/L yeast extract, 20 g/L tryptone, 13.4 g/L YNB, 100 mM potassium phosphate buffer pH 6.0 and 1% (v/v) methanol) at 25°C. And Basal salt medium (BSM) (2.67 g/L phosphoric acid, 0.93 g/L $CaSO_4$, 18.2 g/L K_2SO_4, 14.9 g/L $MgSO_4 \cdot 7H_2O$, 4.13 g/L KOH, 40 g/L glycerol and 4.35 mL/L PTM1) and the trace metal solution PTM1 (6 g/L $CuSO_4 \cdot 5H_2O$, 0.08 g/L NaI, 3 g/L $MnSO_4 \cdot H_2O$, 0.2 g/L $Na_2MoO_4 \cdot 2H_2O$, 0.02 g/L H_3BO_3, 0.5 g/L $CoCl_2 \cdot 6H_2O$, 20 g/L $ZnCl_2$, 65 g/L $FeSO_4 \cdot 7H_2O$, 0.2 g/L biotin, 5 mL/L H_2SO_4) were used for fed-batch fermentation with *P. pastoris*, and add 2 g/L of histidine to the BSM medium when necessary.

NMR and HRMS Characterization of the Products

All Nuclear Magnetic Resonance (NMR) spectra were recorded in DMSO-*d6* with Bruker AVANCE AV400 spectrometer. Those NMR data were processed and analyzed with MestReNova 14.0 (Supplementary Figs. 14-55). The correlation experiments included ^{1}H, ^{13}C, ^{1}H,^{1}H-COSY, ^{1}H,^{1}H-NOESY, ^{1}H,^{13}C-HSQC and ^{1}H,^{13}C-HMBC. All High-Resolution Mass Spectrometry (HRMS) data for the new compounds were acquired using an Agilent G6224A mass spectrometer. Those HRMS data were processed and analyzed with Qualitative Navigator B.08.00 (Supplementary Figs. 56-58).

NMR and HR-EMIMS data

15*α*-hydroxy-canrenone

^{1}H NMR (DMSO-d_6, 400 MHz) δ 6.47 (1H, dd, 10.1, 2.1 Hz, H-7), 6.15 (1H, dd, 10.1, 2.6 Hz, H-6), 5.38 (1H, s, H-4), 3.90 (1H, m, H-15), 0.84 (3H, s, H-19), 0.69 (3H, s, H-18).

^{13}C NMR (DMSO-d_6, 100 MHz) δ 198.1 (C-3), 176.3 (C-22), 163.1 (C-5), 141.7 (C-7), 126.6 (C-6), 122.9 (C-4), 92.9 (C-17), 69.9 (C-15), 53.8 (C-14), 49.7 (C-9), 46.9 (C-16), 46.5 (C-13), 37.2 (C-8), 35.6 (C-10), 33.7 (C-2), 33.5 (C-1), 31.2 (C-12), 30.8 (C-20), 28.9 (C-21), 19.7 (C-11), 16.1 (C-19), 15.7 (C-18).

12*β*-hydroxy-canrenone

^{1}H NMR (DMSO-d_6, 400 MHz) δ 6.21 (1H, dd, 9.7, 2.5 Hz, H-6), 6.15 (1H, dd, 9.7, 1.7 Hz, H-7), 5.64 (1H, s, H-4), 4.62 (1H, br s, 12-OH), 3.61 (1H, dd, 10.6, 4.4 Hz, H-12), 1.07 (3H, s, H-19), 0.90 (3H, s, H-18).

^{13}C NMR (DMSO-d_6, 100 MHz) δ 198.1 (C-3), 176.7 (C-22), 162.8 (C-5), 139.9 (C-7), 127.9 (C-6), 123.2 (C-4), 94.9 (C-17), 70.9 (C-12), 50.0 (C-13), 47.7 (C-9), 45.2 (C-14), 36.6 (C-8), 35.9 (C-16), 35.4 (C-10), 33.6 (C-2), 33.4 (C-1), 30.8 (C-20), 29.8 (C-11), 29.5 (C-21), 21.4 (C-15), 16.0 (C-19), 8.7 (C-18).

HRMS (ESI) m/z: calcd for $C22H29O4^{+}[M+H]^{+}$, 357.2066; found, 357.2059.

15*α*-hydroxy-bisnoralcohol

^{1}H NMR (DMSO-d_6, 400 MHz) δ 5.61 (1H, s, H-4), 4.33 (1H, d, 6.1 Hz, 15-OH), 4.29 (1H, m, 21-OH), 3.75 (1H, m, H-15), 3.36 (1H, m, H-21a), 3.04 (1H, m, 4.5 Hz, H-21b), 1.15 (3H, s, H-19), 0.93 (1H, d, 5.5 Hz, H-22), 0.69 (3H, s, H-18).

^{13}C NMR (DMSO-d_6, 100 MHz) δ 198.0 (C-3), 171.4 (C-5), 122.9 (C-4), 71.8 (C-15), 65.6 (C-21), 61.7 (C-14), 53.6 (C-9), 49.9 (C-17), 42.8 (C-13), 40.2 (C-16), 39.5 (C-12), 38.2 (C-20), 38.2 (C-10), 35.2 (C-1), 34.9 (C-8), 33.6 (C-2), 32.2 (C-6), 32.0 (C-7), 20.6 (C-11), 17.0 (C-19), 16.9 (C-22), 13.2 (C-18).

HRMS (ESI) m/z: calcd for $C22H35O3^{+}[M+H]^{+}$, 347.2586; found, 347.2571.

12*β*-hydroxy-bisnoralcohol

^{1}H NMR (DMSO-d_6, 400 MHz) δ 5.62 (1H, s, H-4), 4.41 (1H, d, 5.1 Hz, 12-OH), 4.21 (1H, t, 5.1 Hz, 21-OH), 3.48 (1H, m, H-21a), 3.22 (1H, dt, 10.2, 4.7 Hz, H-12), 3.11 (1H, ddd, 9.9, 7.6, 4.5 Hz, H-21b), 1.13 (3H, s, H-19), 1.02 (1H, d, 6.8 Hz, H-22), 0.65 (3H, s, H-18).

^{13}C NMR (DMSO-d_6, 100 MHz) δ 198.1 (C-3), 170.9 (C-5), 123.3 (C-4), 76.9 (C-12), 65.3 (C-21), 55.0 (C-17), 53.1 (C-14), 52.0 (C-9), 47.0 (C-13), 38.0 (C-10), 35.3 (C-20), 35.2 (C-1), 34.0 (C-8), 33.6 (C-2), 32.1 (C-6), 31.2 (C-7), 31.1 (C-11), 24.0 (C-16), 23.4 (C-15), 19.4 (C-22), 16.8 (C-19), 8.0 (C-18).

HRMS (ESI) m/z: calcd for $C22H35O3^{+}[M+H]^{+}$, 347.2586; found, 347.2572.

12*β*, 17*α*-dihydroxy-progesterone

^{1}H NMR (DMSO-d_6, 400 MHz) δ 5.63 (1H, s, H-4), 5.15 (1H, s, 17-OH), 4.40 (1H, d, 5.2 Hz, 12-OH), 4.21 (1H, t, 5.1 Hz, 21-OH), 3.89 (1H, dt, 10.6, 4.9 Hz, H-12), 2.27 (3H, s, H-21), 1.13 (3H, s, H-19), 0.55 (3H, s, H-18).

^{13}C NMR (DMSO-d_6, 100 MHz) δ 213.6 (C-20), 198.0 (C-3), 170.6 (C-5), 123.3 (C-4), 88.6 (C-17), 68.2 (C-12), 53.1 (C-13), 51.8 (C-9), 49.1 (C-14), 38.0 (C-10), 35.2 (C-1), 34.7 (C-16), 34.1 (C-8), 33.6 (C-2), 32.1 (C-6), 31.5 (C-7), 30.3 (C-11), 27.6 (C-21), 23.1 (C-15), 16.9 (C-19), 9.0 (C-18).

15*α*-hydroxy-testosterone

^{1}H NMR (DMSO-d_6, 400 MHz) δ 5.61 (1H, s, H-4), 3.82 (1H, td, 9.4, 3.4 Hz, H-15), 3.60 (1H, t, 8.8 Hz, H-17),1.14 (3H, s, H-19), 0.67 (3H, s, H-18).

^{13}C NMR (DMSO-d_6, 100 MHz) δ 198.5 (C-3), 171.8 (C-5), 123.4 (C-4), 77.8 (C-17), 71.3 (C-15), 58.0 (C-14), 54.2 (C-9), 44.0 (C-13), 43.0 (C-16), 38.8 (C-10), 37.1 (C-12), 35.7 (C-1), 35.5 (C-8), 34.1 (C-2), 32.6 (C-6), 32.6 (C-7), 20.7 (C-11), 17.5 (C-19), 13.2 (C-18).

15*α*-hydroxy-androstenedione

^{1}H NMR (DMSO-d_6, 400 MHz) δ 5.63 (1H, s, H-4), 4.21 (1H, m, H-15), 1.17 (3H, s, H-19), 0.86 (3H, s, H-18).

^{13}C NMR (DMSO-d_6, 100 MHz) δ 216.3 (C-17), 197.9 (C-3), 170.8 (C-5), 123.0 (C-4), 68.7 (C-15), 56.6 (C-14), 53.4 (C-9), 49.6 (C-13), 46.0 (C-16), 38.3 (C-10), 35.2 (C-1), 34.9 (C-8), 33.7 (C-2), 32.1 (C-6), 31.8 (C-7), 31.2 (C-12), 19.9 (C-11), 17.1 (C-19), 14.9 (C-18).

Supplementary Tables

Supplementary Table 1. Diverse electronic states in the QM model of CYP68J5_fg (Cpd I) with substrate (1) bound at pose 12.

entry	multiplicity	spin				E_{cor} (kcal/mol)
		Fe	O	S(CYS)	N(HEM)	
1	II	1.25	0.84	-0.78	0.29	3.2
2	IV	1.18	0.83	0.84	0.41	0.0
3	IV	3.22	0.60	-0.80	0.83	10.8
4	VI	3.12	0.56	0.80	0.82	11.0

Supplementary Table 2. Diverse electronic states in the QM model of CYP68J5_fg (Cpd I) with substrate (1) bound at pose 15.

entry	multiplicity	spin				E_{cor} (kcal/mol)
		Fe	O	S(CYS)	N(HEM)	
1	II	1.24	0.85	-0.83	-0.04	0.1
2	IV	1.15	0.87	0.74	0.21	0.0
3	IV	3.23	0.60	-0.75	0.00	7.1
4	VI	3.11	0.58	0.72	0.12	9.3

Supplementary Figures

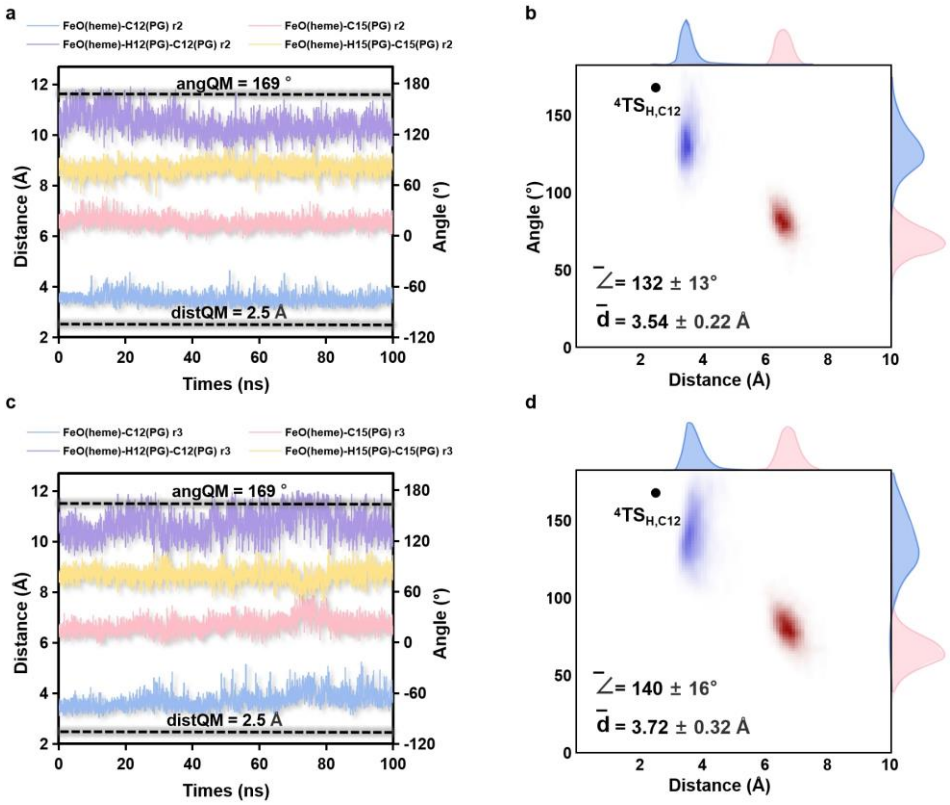

Supplementary Figure 1. MD simulations of W12M5 in pose 12 in the reaction with 1. a, **c**, Plots of the C12, C15 (**1**)···O=Fe distances (y primary axis) and the O(Fe=O)-(**1**)-H(12C, 15C)-(**1**)-C(12, 15) angles (y secondary axis) along the simulation time (x axis) for the second (**a**) and third (**c**) replicas. **b**, **d**, Conformational population analysis of the prereaction states in the 100 ns MD simulation trajectories.

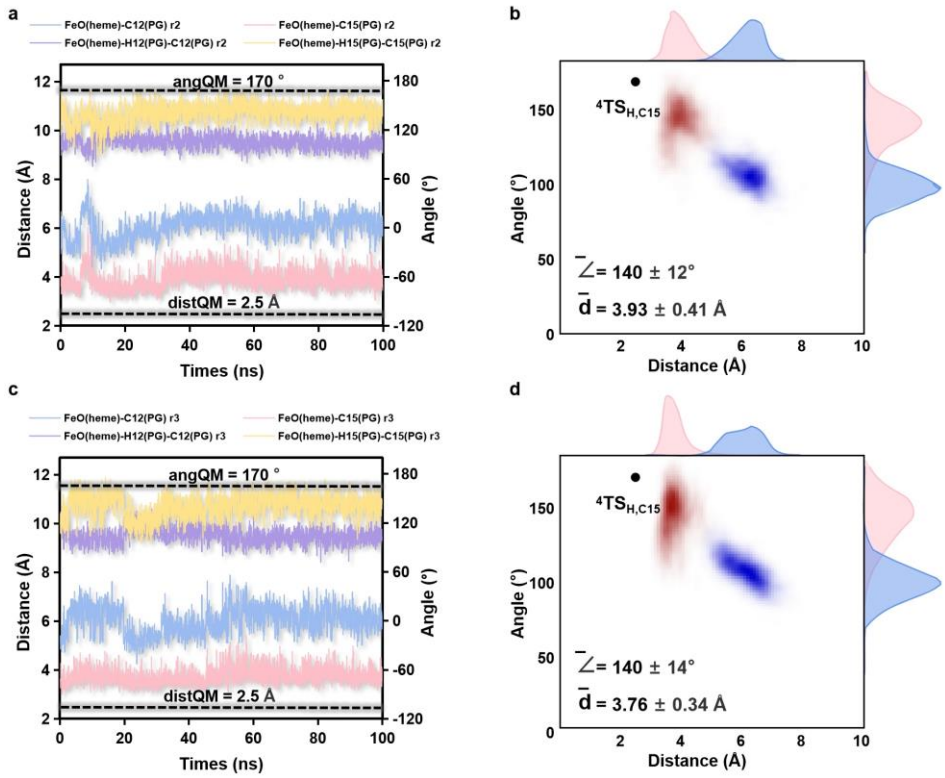

Supplementary Figure 2. MD simulations of W15M4 in pose 15 in the reaction with 1. a, **c**, Plots of the C12, C15 (**1**)···O=Fe distances (y primary axis) and the O(Fe=O)-(**1**)-H(12C, 15C)-(**1**)-C(12, 15) angles (y secondary axis) along the simulation time (x axis) for the second (**a**) and third (**c**) replicas. **b**, **d**, Conformational population analysis of the prereaction states in the 100 ns MD simulation trajectories.

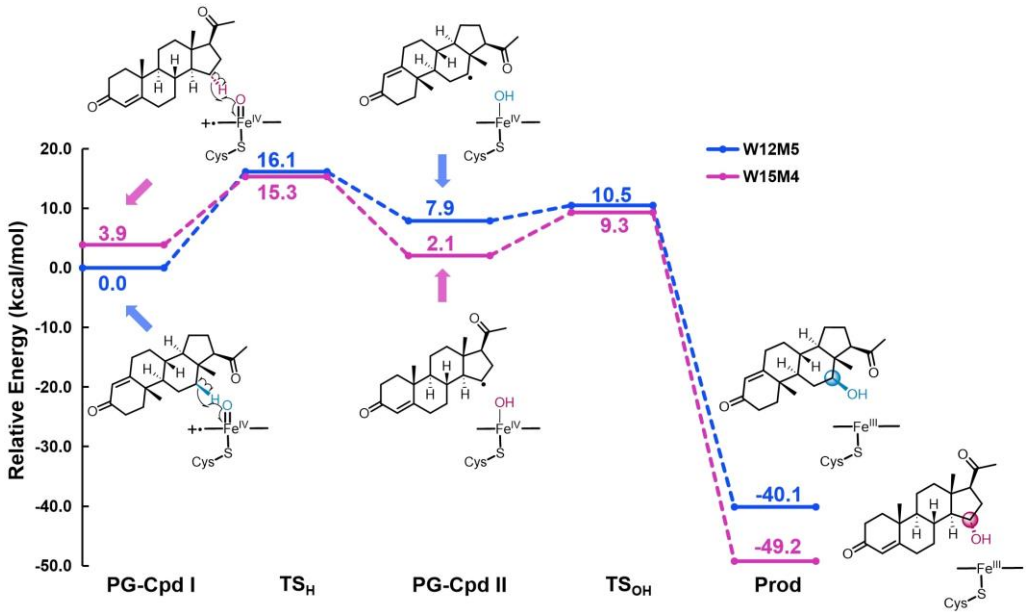

Supplementary Figure 3. Potential energy profiles for the CYP68J5_fg-catalyzed C(12,15)-hydroxylation of 1. Abbreviations indicate the Cpd I and substrate PG complex (**PG-Cpd I**), the TS for hydrogen-atom transfer from PG to heme Fe=O species (**TS$_H$**), the intermediate including Fe-OH species and the PG radical (**PG-Cpd II**), the TS for hydroxyl radical rebound from Cpd II to PG (**TS$_{OH}$**), and the hydroxylated substrate product intermediate (**Prod**).

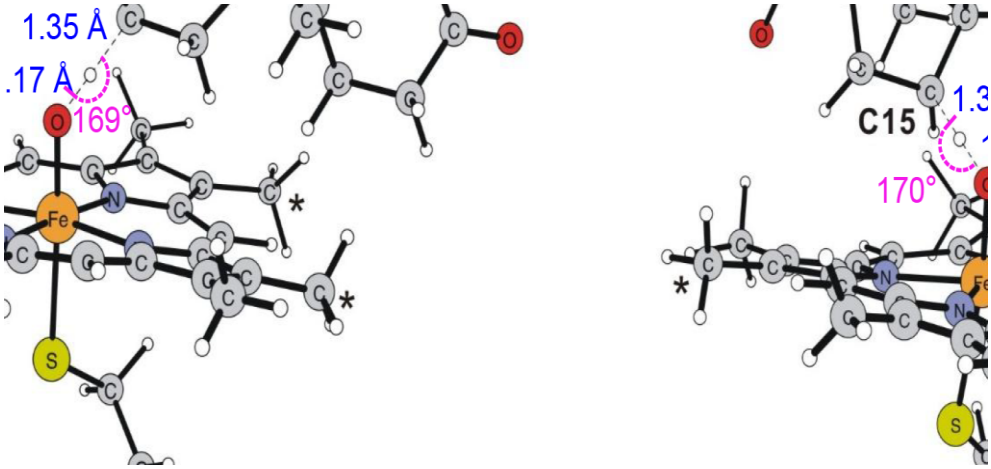

Supplementary Figure 4. QM-optimized transition-state structures for C(12,15)-H abstraction in 1. Key geometrical parameters are indicated with dashed lines. Asterisks indicate the atoms fixed in their X-ray positions.

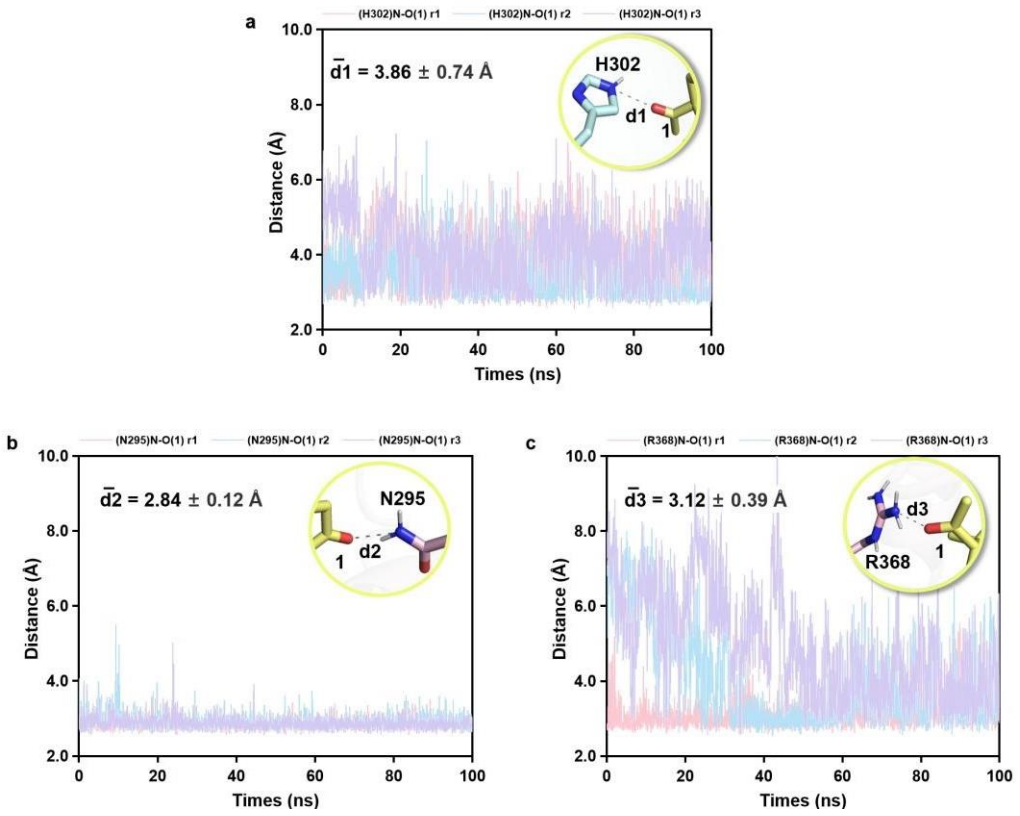

Supplementary Figure 5. Plot of the distances of H-bonds for three independent MD simulations with 1 bound in CYP68J5_fg mutants, W12M5 and W15M4. a, (H302)N···O(PG) in W12M5; **b**, (N295)N···O(PG) in W15M4; **c**, (R368)N···O(PG) in W15M4. Mean values (in Å) and standard deviations for the whole MD replica dataset are shown.

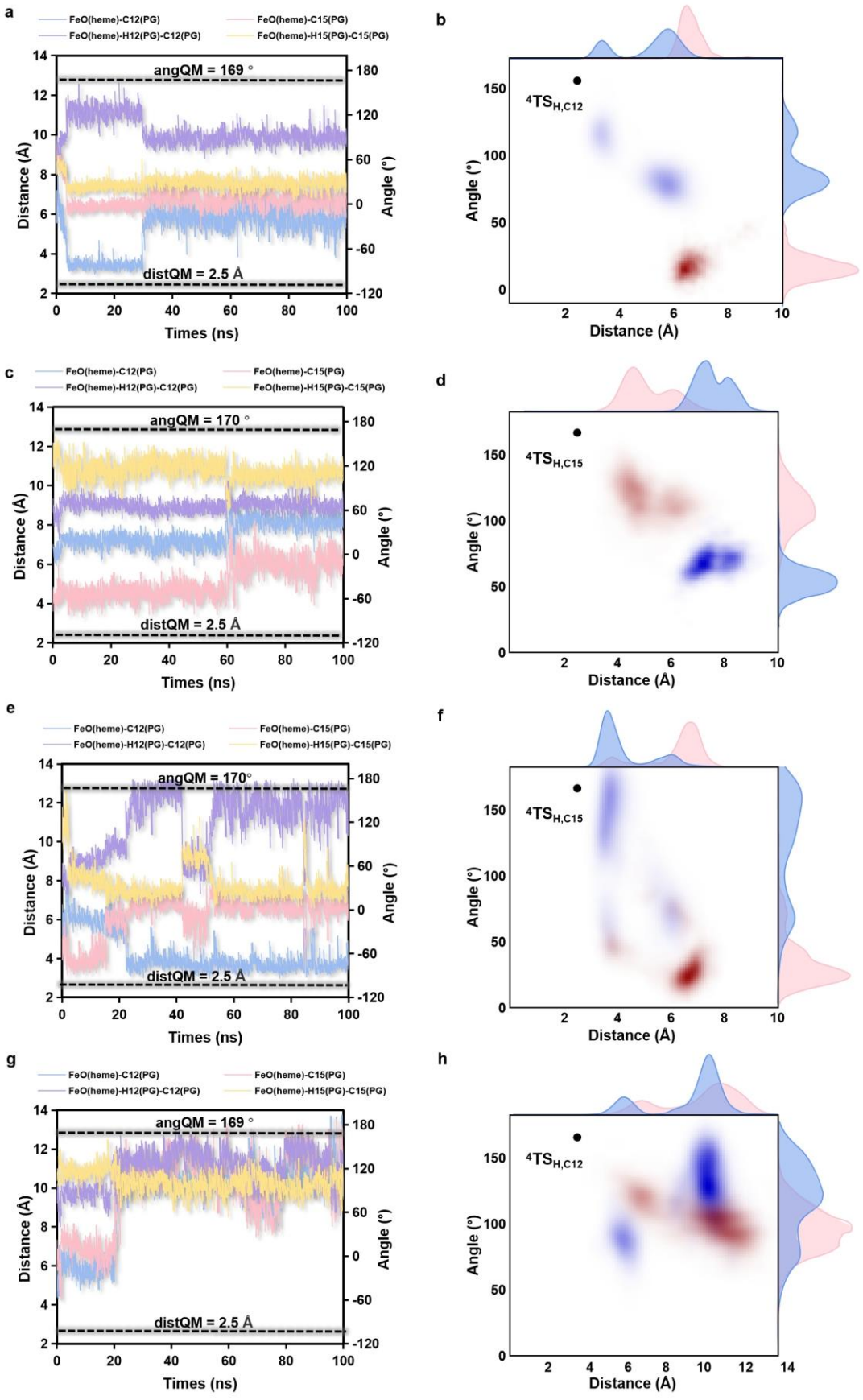
a
FeO(heme)-C12(PG)
FeO(heme)-C15(PG)
FeO(heme)-H12(PG)-C12(PG)
FeO(heme)-H15(PG)-C15(PG)
angQM = 169 °
distQM = 2.5 Å
Distance (Å)
Angle (°)
Times (ns)
b
$^4TS_{H,C12}$
Angle (°)
Distance (Å)
c
FeO(heme)-C12(PG)
FeO(heme)-C15(PG)
FeO(heme)-H12(PG)-C12(PG)
FeO(heme)-H15(PG)-C15(PG)
angQM = 170 °
distQM = 2.5 Å
Distance (Å)
Angle (°)
Times (ns)
d
$^4TS_{H,C15}$
Angle (°)
Distance (Å)
e
FeO(heme)-C12(PG)
FeO(heme)-C15(PG)
FeO(heme)-H12(PG)-C12(PG)
FeO(heme)-H15(PG)-C15(PG)
angQM = 170°
distQM = 2.5 Å
Distance (Å)
Angle (°)
Times (ns)
f
$^4TS_{H,C15}$
Angle (°)
Distance (Å)
g
FeO(heme)-C12(PG)
FeO(heme)-C15(PG)
FeO(heme)-H12(PG)-C12(PG)
FeO(heme)-H15(PG)-C15(PG)
angQM = 169 °
distQM = 2.5 Å
Distance (Å)
Angle (°)
Times (ns)
h
$^4TS_{H,C12}$
Angle (°)
Distance (Å)

Supplementary Figure 6. MD simulations of CYP68J5_fg and its variants in the non-productive position with 1. a, **c**, **e, g,** Distances determined between the oxygen atom of the Fe=O and the C(12,15) atom of **1** (x axis) and angles formed by O(Fe=O)-(**1**)-H(C12,15)-(**1**)-C(12,15) (y axis) in CYP68J5_fg (Pose 12, 15) (**a**, **c**), W12M5 (Pose 15) (**e**) and W15M4 (Pose 12) (**g**) along the whole simulation time. **b**, **d**, **f**, **h**, Conformational population analysis of the prereaction states of CYP68J5_fg (**b**, **d**), W12M5 (**f**) and W15M4 (**h**) in the 100 ns MD simulation trajectories.

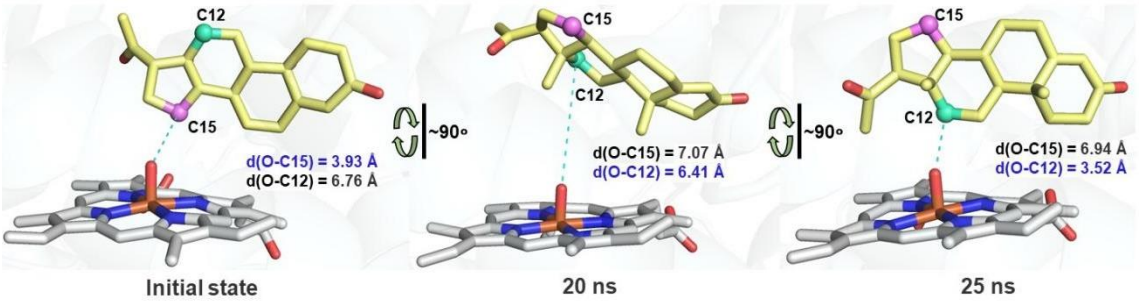

Supplementary Figure 7. Representative Snapshots from MD Simulations of the W12M5-1 Complex. Each snapshot illustrates the spatial arrangement of substrate **1** (yellow) relative to the heme iron-oxygen (gray).

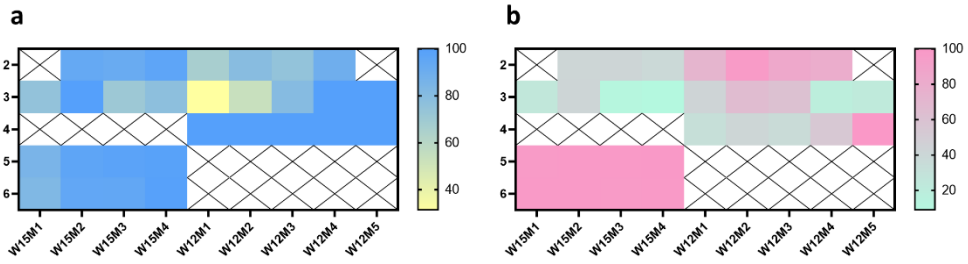

Supplementary Figure 8. The selectivity and activity results of different mutants towards various substrates were screened using 96-well plates. a, Selectivity results of different mutants of CYP68J5_fg towards substrates **2**, **3**, **4**, **5** and **6**. **b**, Conversion rates of different mutants of CYP68J5_fg towards substrates **2**, **3**, **4**, **5** and **6**. Abbreviation for substrate: Canrenone (**2**), Bisnoralcohol (**3**), 17α-Hydroxyprogesterone (**4**), Testosterone (**5**), Androstenedione (**6**).

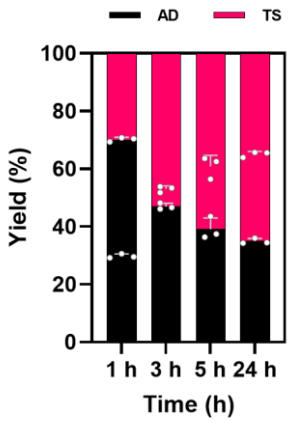

Supplementary Figure 9. Bioconversion of 1 mM AD by AYR1 from *P. pastoris* in *E. coli* [2]. Reaction conditions: 3 mL *E. coli* cell lysate containing 1 mM AD, 3% (w/v) glucose, 1 U/mL glucose dehydrogenase (GDH), and 0.2 mM $NAD(P)^+$ cofactor. The data shown in Supplementary Figure 9 are presented as the mean ± s.d. of three biological replicates. Source data are provided as a Source Data file.

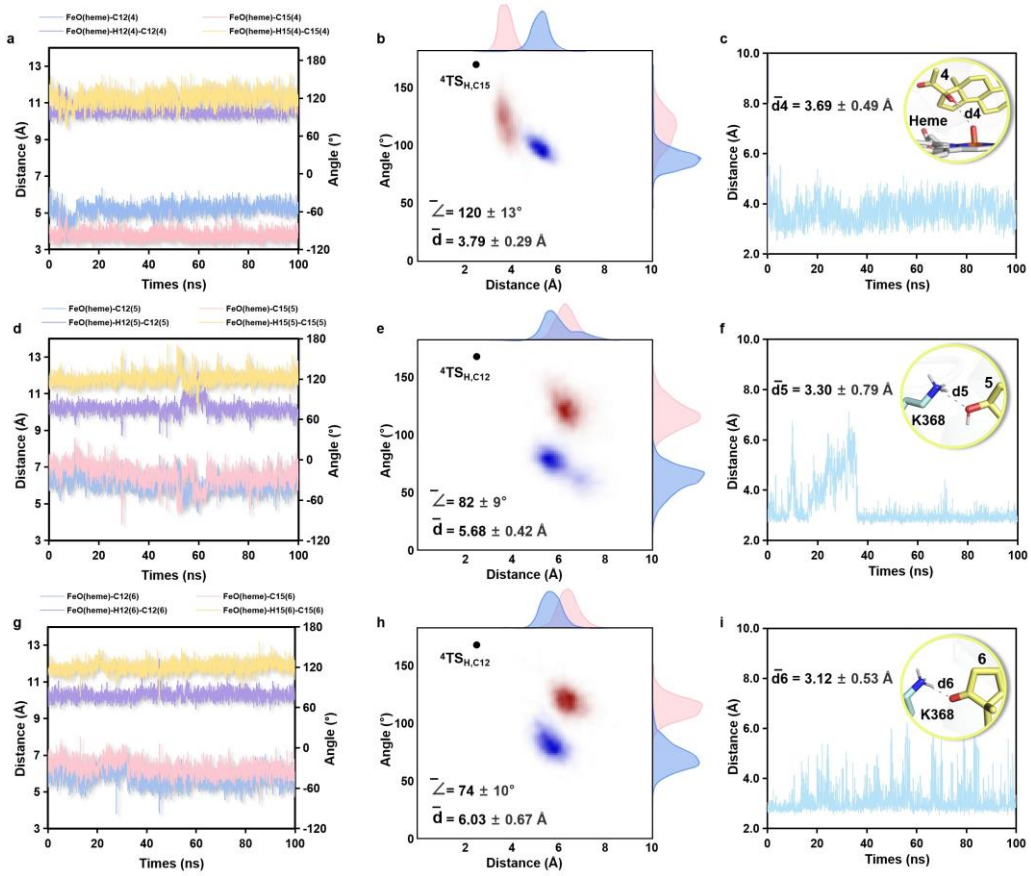

Supplementary Figure 10. MD simulations of CYP68J5_fg variants with steroids. a, **d**, **g**, Plots of the C12, C15(**1**)···O=Fe distances (y primary axis) and the O(Fe=O)-(**steroids**)-H(12C, 15C)-(**steroids**)-C(12, 15) angles (y secondary axis) along the simulation time (x axis) for W15M4 bound with **4** (**a**) and W12M5 bound with **5** (**d**) and **6** (**g**). **b**, **e**, **h**, Conformational population analysis of the prereaction states of W15M4 bound with **4** (**b**) and W12M5 bound with **5** (**e**) and **6** (**h**) in the 100 ns MD simulation trajectories. **c**, **f**, **i**, H-bond distance plots. (**c**) O(Fe=O)···O(**4**) in W12M5; (**f**) (K368)N···O(**5**) in W15M4; (**i**) (K368)N···O(**6**) in W15M4.

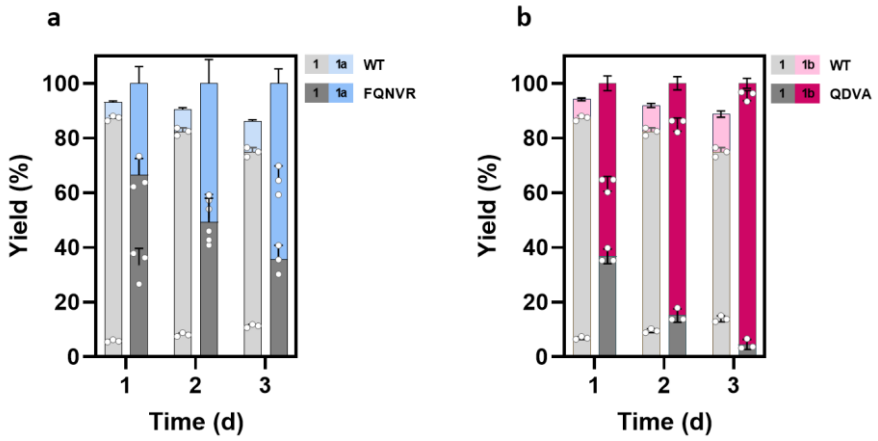

Supplementary Figure 11. Conversion of 1 by the CYP68J5_fg mutants in *P. pastoris*. **a**, Result of substrate and product yield for **1** conversion by strain GS115-FQNVR. **b**, Result of substrate and product yield for **1** conversion by strain GS115-QDVA. Reaction conditions: *P. pastoris* cells were used for fermentation, the final concentration of **1** was 2 mM, with reaction times of 1, 2, and 3 days. All experiments were replicated three times. The data shown in **a**, **b** are presented as the mean ± s.d. of three biological replicates. Source data are provided as a Source Data file.

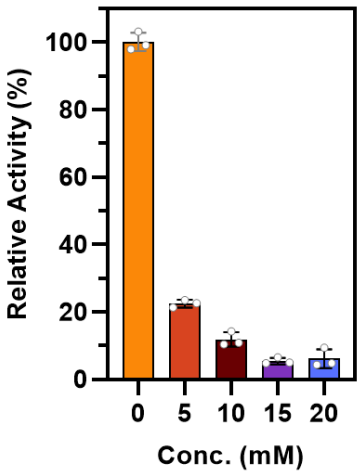

Supplementary Figure 12. Relative activity of GS115-W12M5 after 24 h reaction with simultaneous addition of varying concentrations of 1a and 5 mM substrate 1. The concentrations on the x-axis represent the initial concentrations of compound **1a** (0, 5, 10, 15, 20 mM) added simultaneously with a fixed concentration (5 mM) of substrate **1** at the start of the reaction. The data shown in Supplementary Figure 12 are presented as the mean ± s.d. of three biological replicates. Source data are provided as a Source Data file.

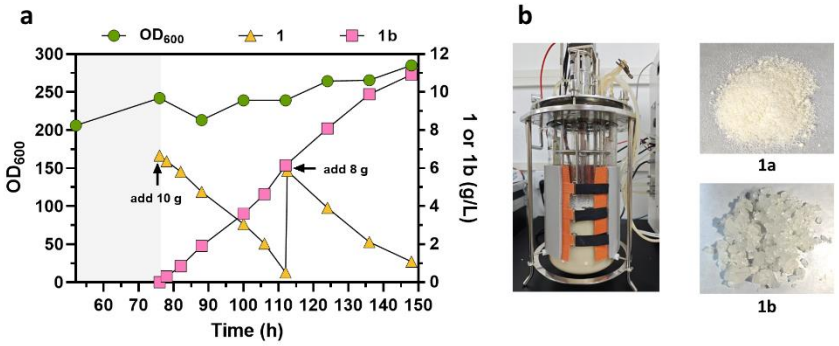

Supplementary Figure 13. Conversion of 1 by the GS115-W15M4 in *P. pastoris*. a, **1b** production by the GS115-W15M4 in a 5-L fermenter induced by methanol with 18 g substrate **1**. **b**, The final state of GS115-W15M4 fermentation. Compounds **1a** and **1b** were isolated from the fermentation broth through sequential purification steps. Source data are provided as a Source Data file.

Supplementary Figures for NMR

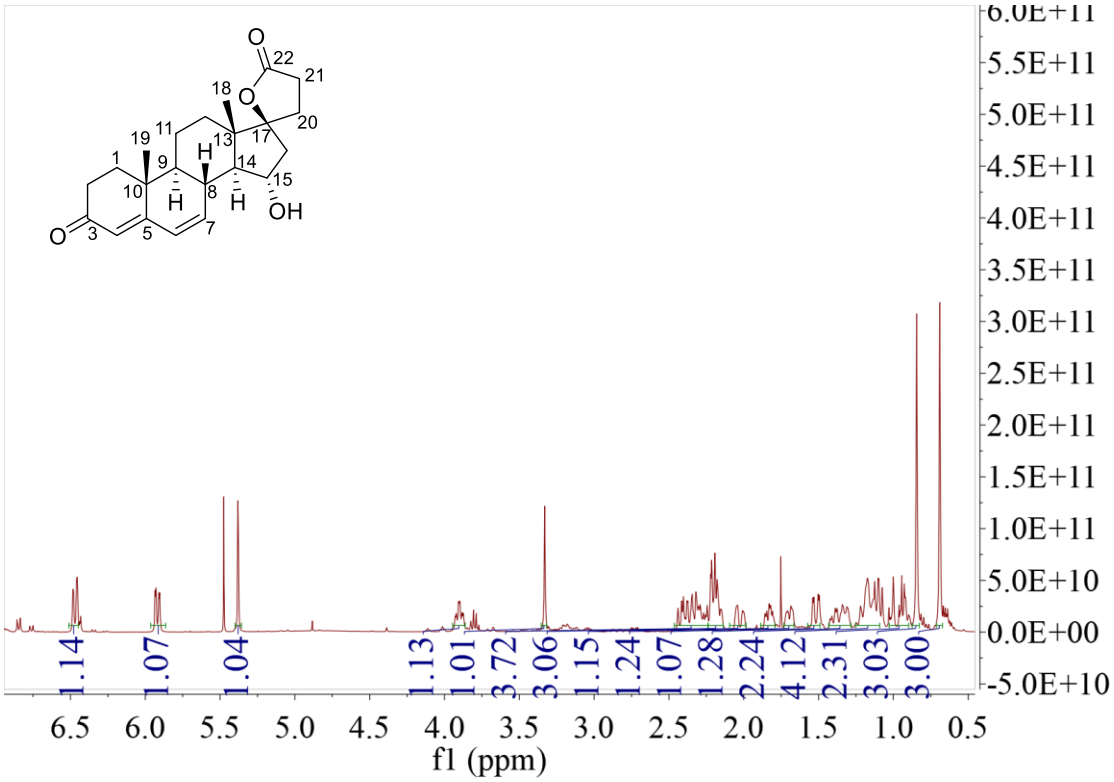

Supplementary Figure 14. ^{1}H NMR spectrum of 15α-hydroxy-canrenone in DMSO-d_6 (400 MHz).

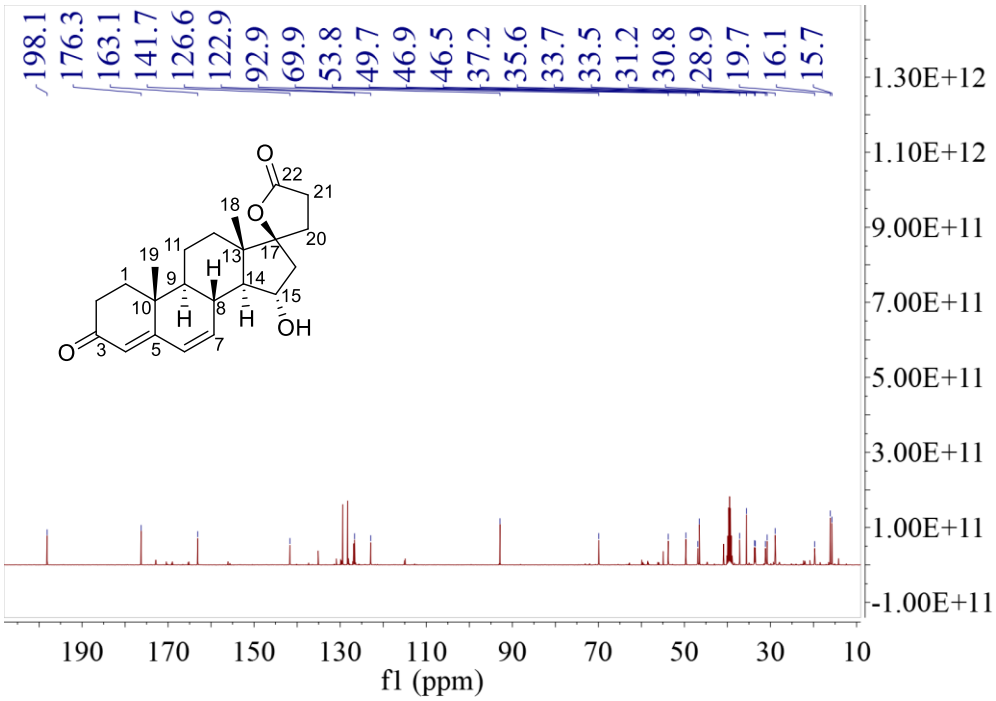

Supplementary Figure 15. ^{13}C NMR spectrum of 15α-hydroxy-canrenone in DMSO-*d*6 (100 MHz).

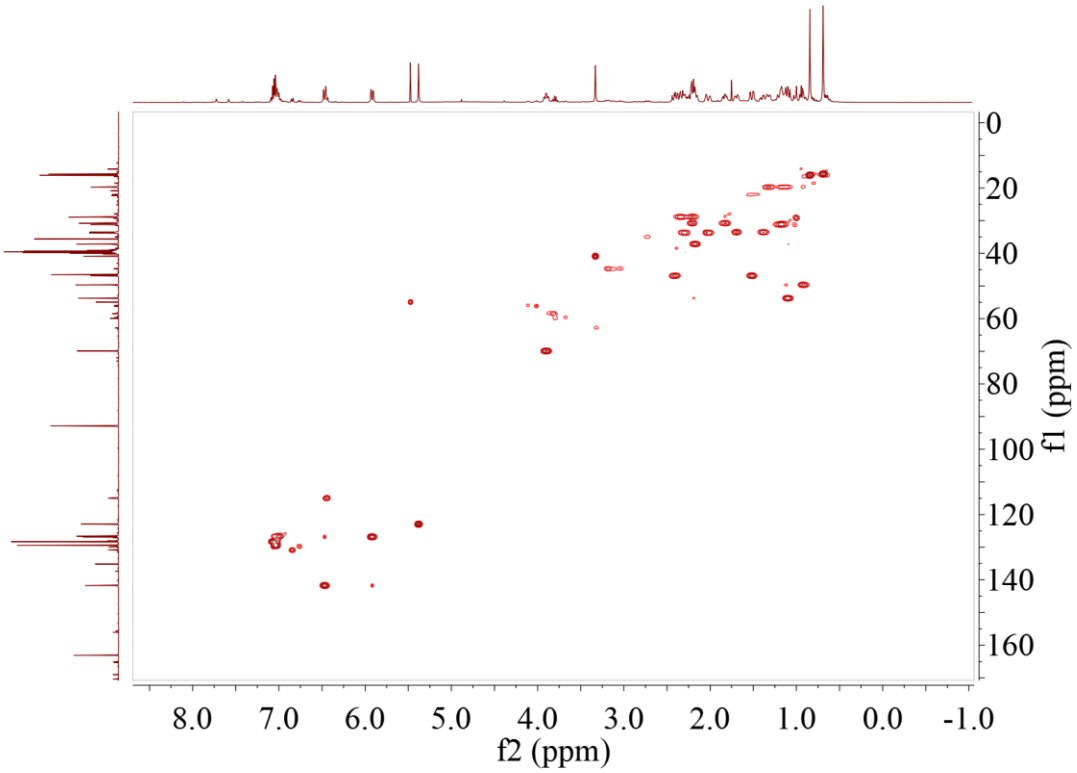

Supplementary Figure 16. HSQC spectrum of 15α-hydroxy-canrenone in DMSO-d_6 (400 MHz for ^{1}H, 100 MHz for ^{13}C).

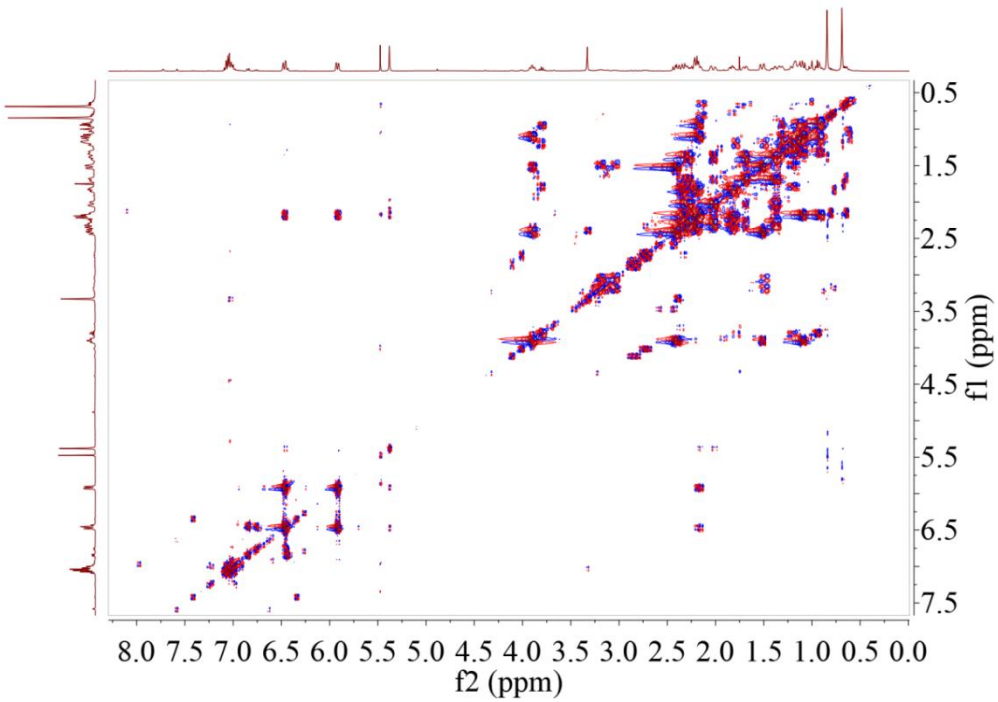

Supplementary Figure 17. ^{1}H-^{1}H COSY spectrum of 15α-hydroxy-canrenone in DMSO-*d*6 (400 MHz for ^{1}H).

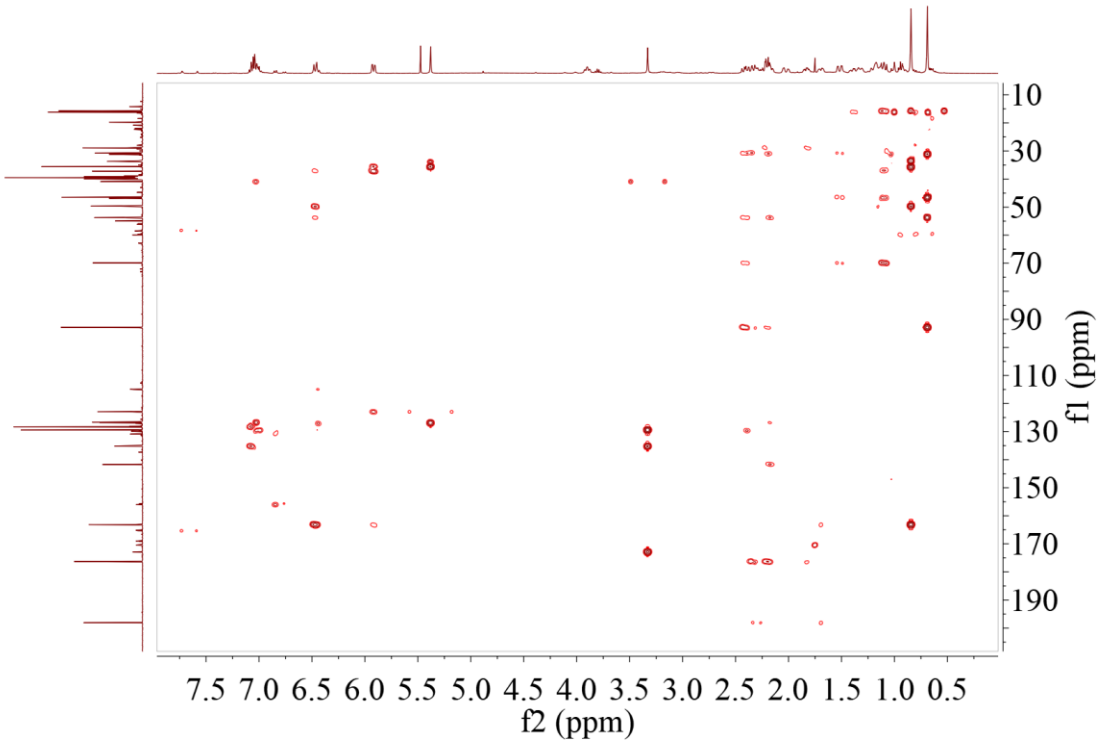

Supplementary Figure 18. HMBC spectrum of 15*α*-hydroxy-canrenone in DMSO-*d*6 (400 MHz for ^{1}H, 100 MHz for ^{13}C).

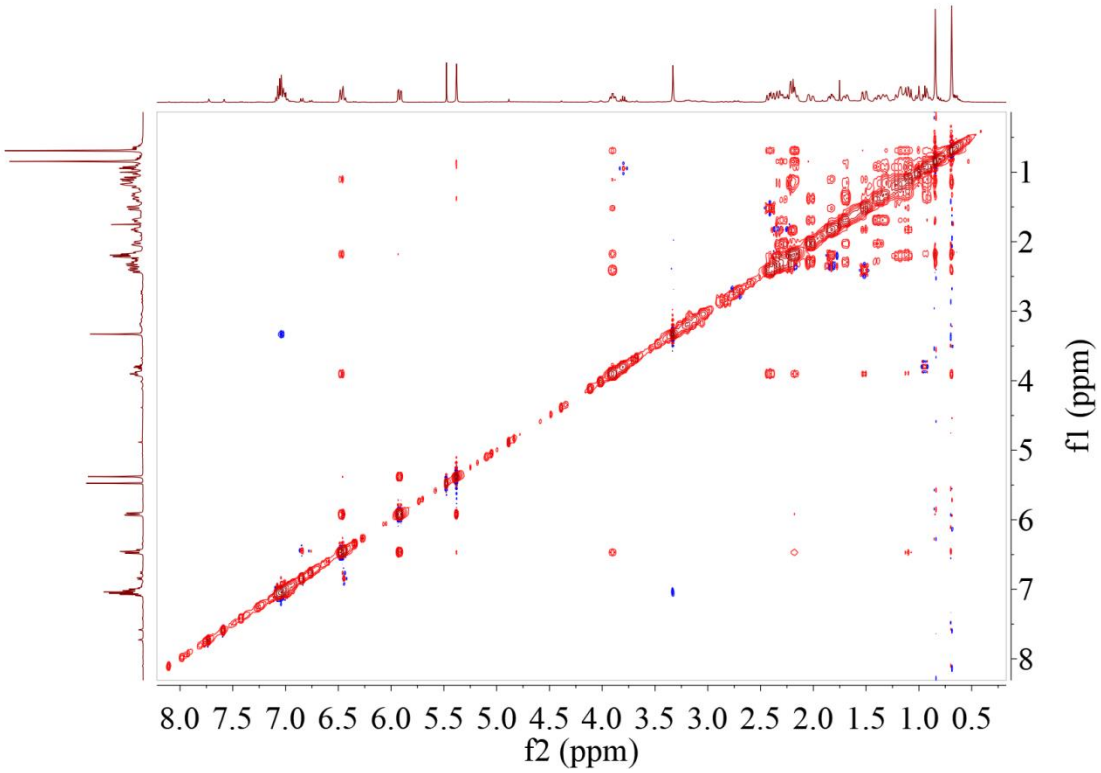

Supplementary Figure 19. NOESY spectrum of 15*α*-hydroxy-canrenone in DMSO-*d*6 (400 MHz).

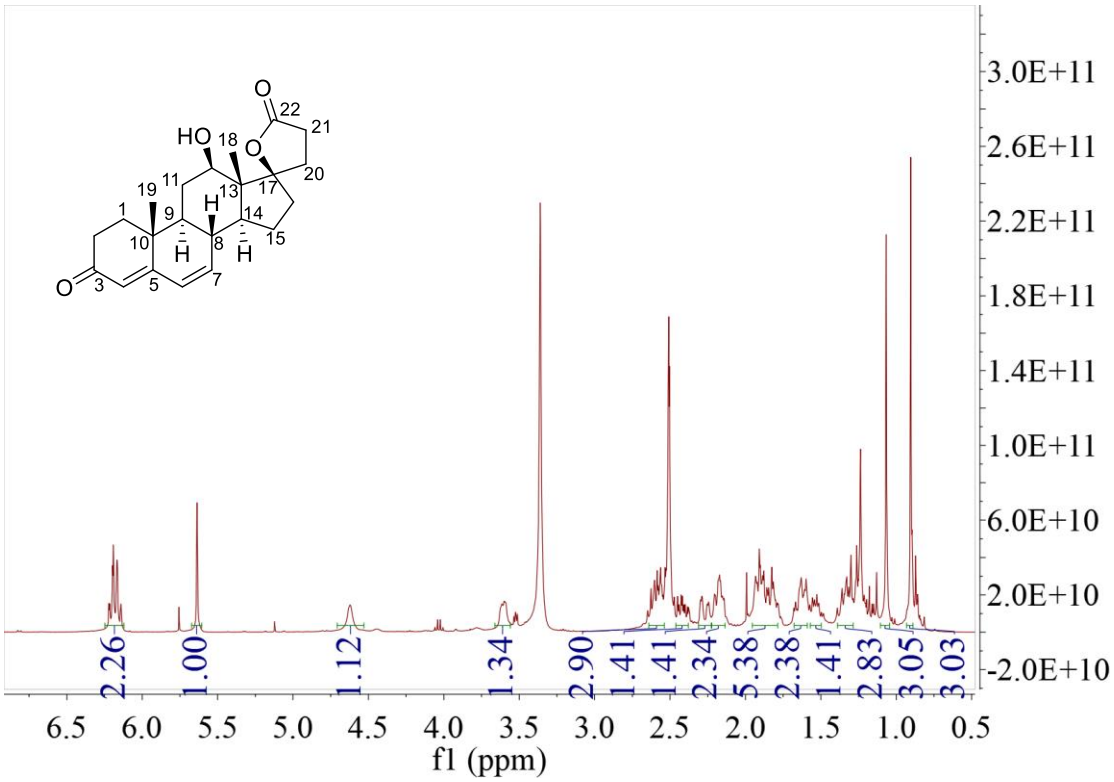

Supplementary Figure 20. ^{1}H NMR spectrum of 12*β*-hydroxy-canrenone in DMSO-*d*6 (400 MHz).

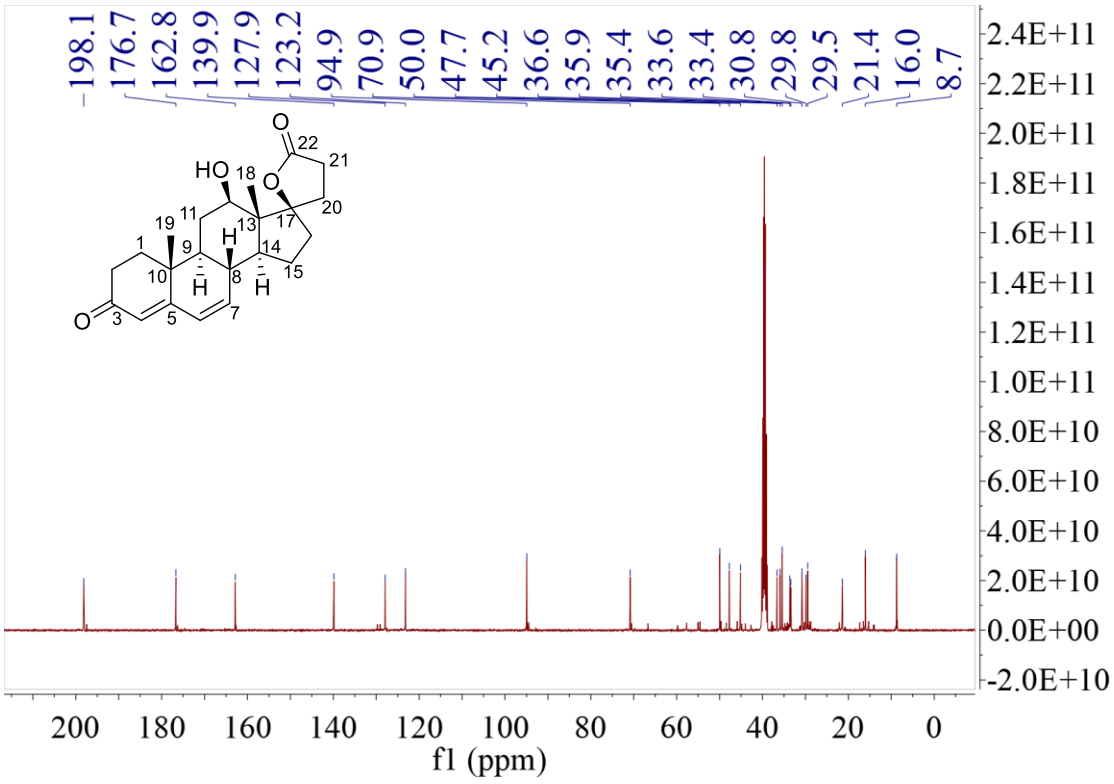

Supplementary Figure 21. ^{13}C NMR spectrum of 12*β*-hydroxy-canrenone in DMSO-*d*6 (100 MHz).

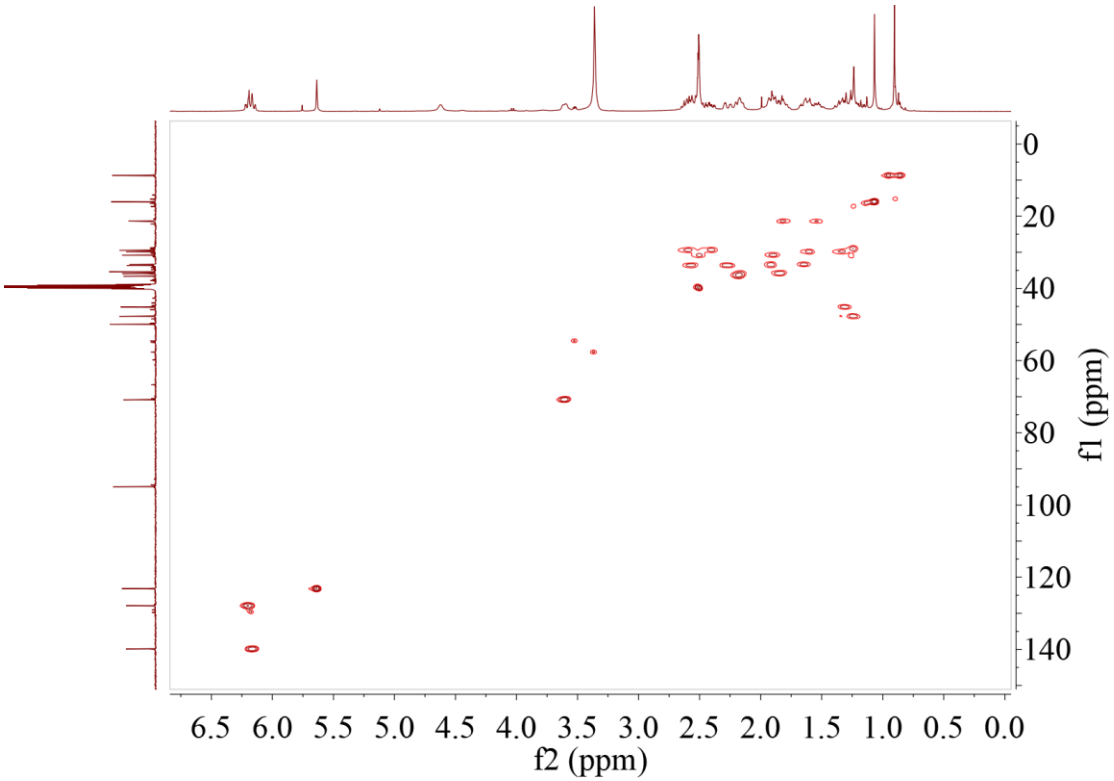

Supplementary Figure 22. HSQC spectrum of 12β-hydroxy-canrenone in DMSO-*d*6 (400 MHz for ^{1}H, 100 MHz for ^{13}C).

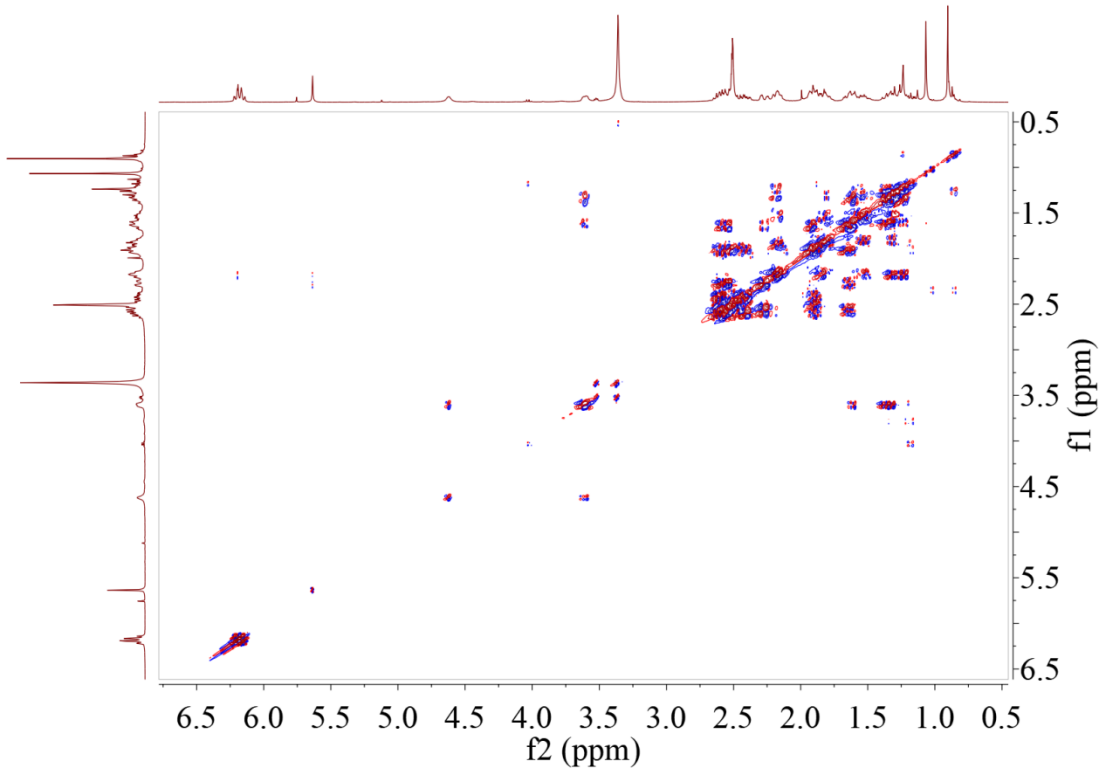

Supplementary Figure 23. ^{1}H-^{1}H COSY spectrum of 12β-hydroxy-canrenone in DMSO-*d*6 (400 MHz).

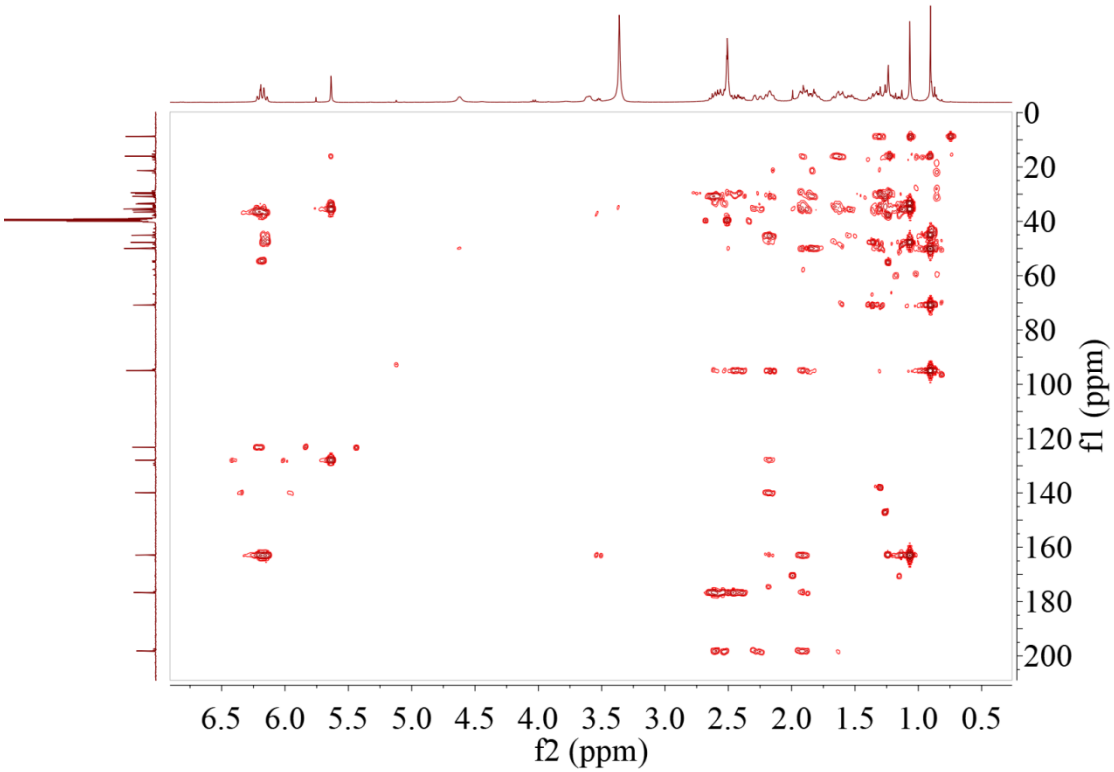

Supplementary Figure 24. HMBC spectrum of 12*β*-hydroxy-canrenone in DMSO-*d*6 (400 MHz for ^{1}H, 100 MHz for ^{13}C).

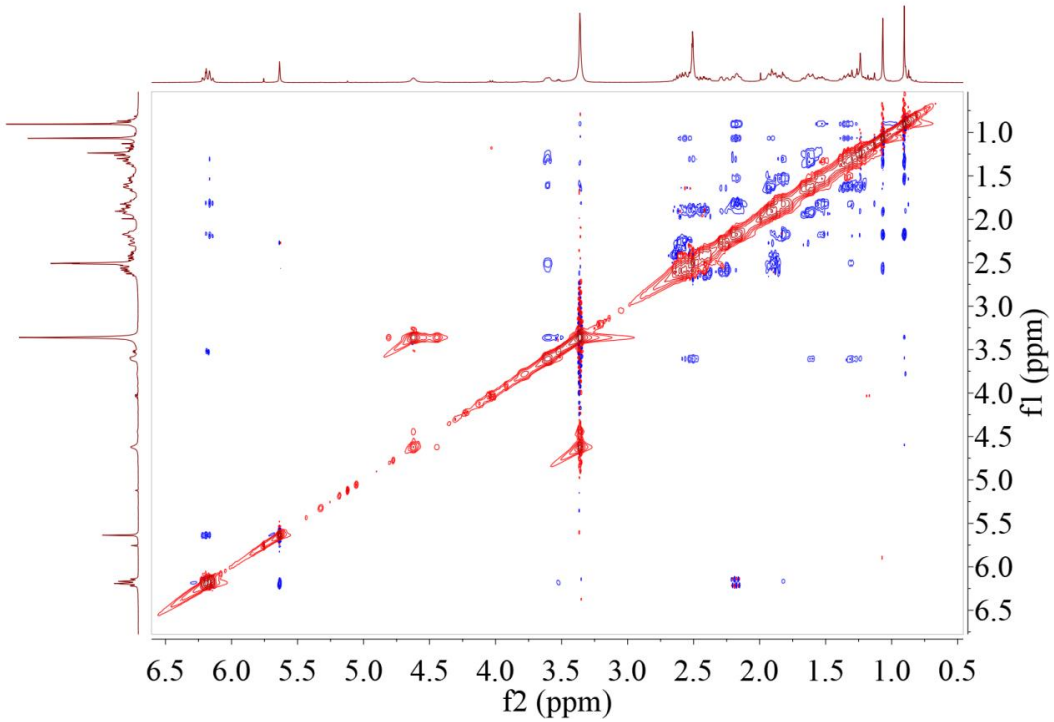

Supplementary Figure 25. NOESY spectrum of 12*β*-hydroxy-canrenone in DMSO-*d*6 (400 MHz).

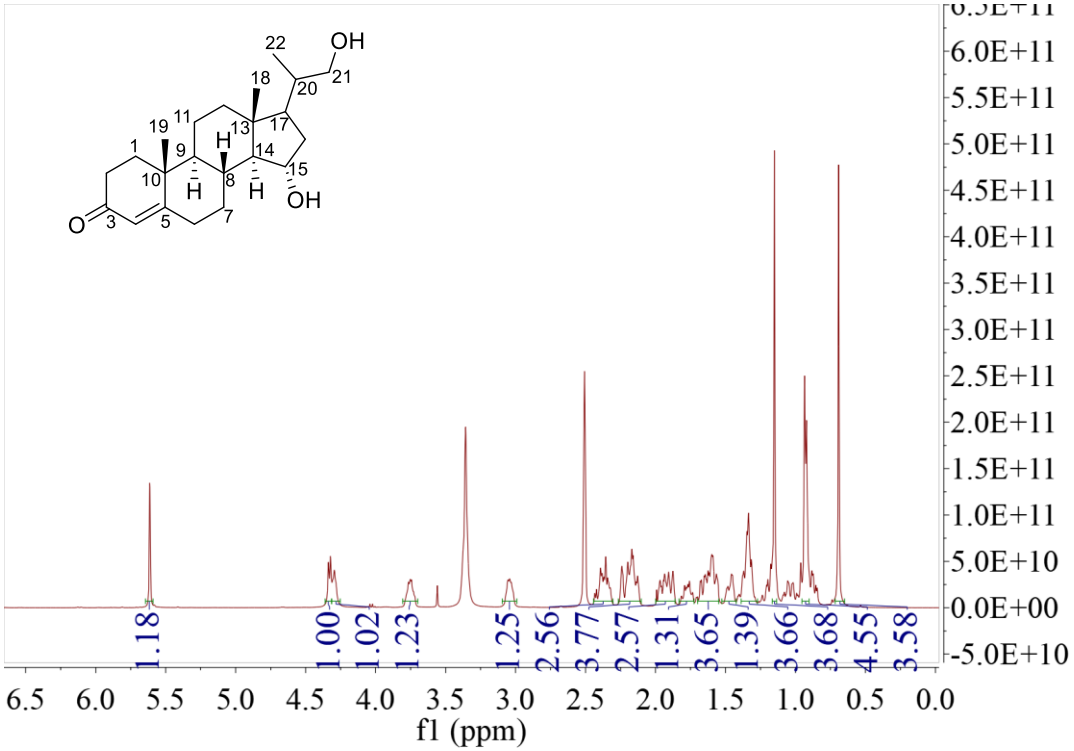

Supplementary Figure 26. [1]H NMR spectrum of 15*α*-hydroxy-bisnoralcohol in DMSO-*d*6 (400 MHz).

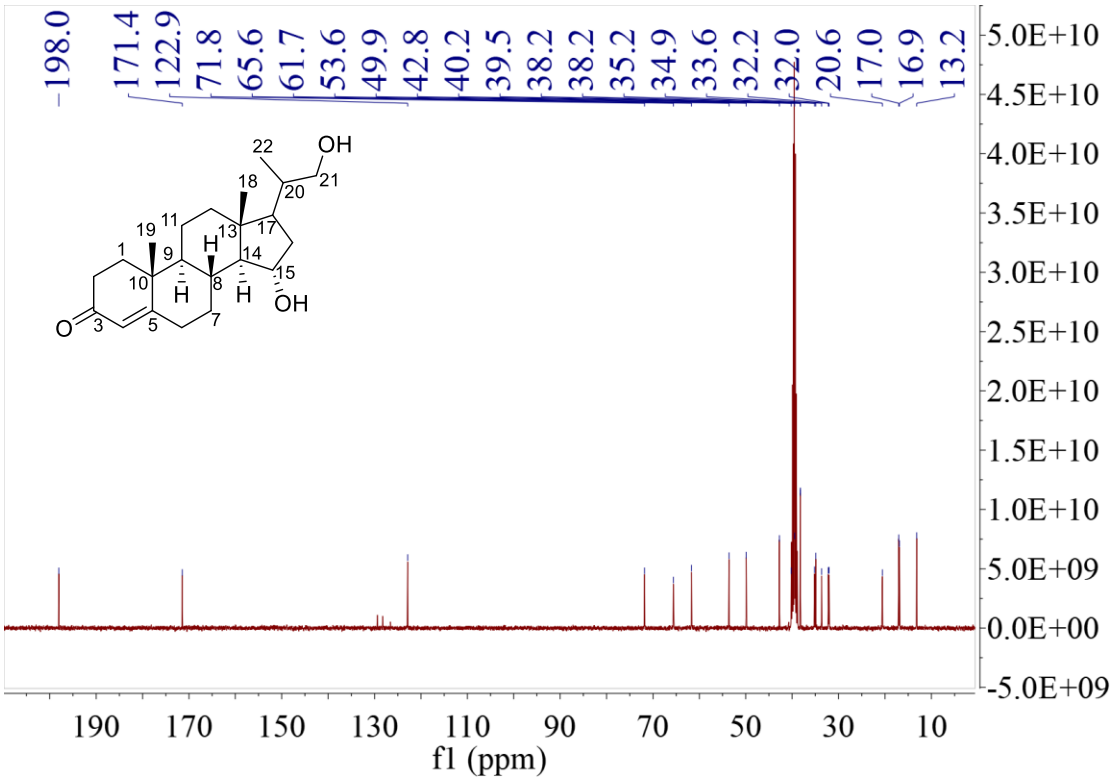

Supplementary Figure 27. [13]C NMR spectrum of 15*α*-hydroxy-bisnoralcohol in DMSO-*d*6 (100 MHz).

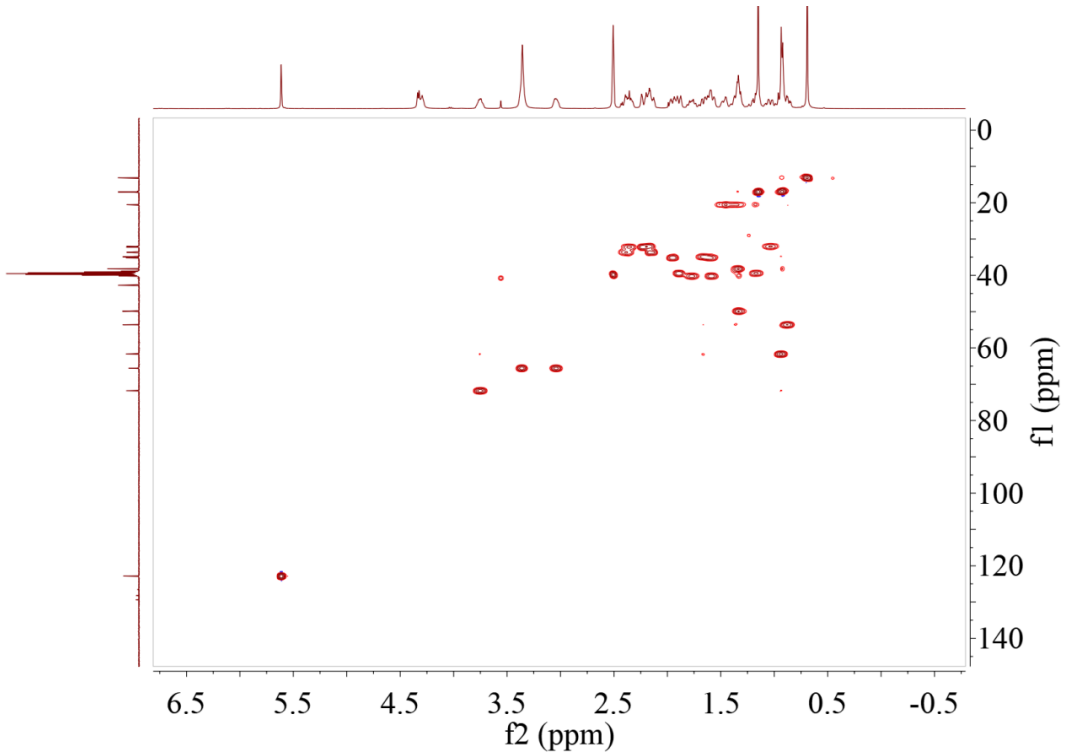

Supplementary Figure 28. HSQC spectrum of 15α-hydroxy-bisnoralcohol in DMSO-*d*6 (400 MHz for ^{1}H, 100 MHz for ^{13}C).

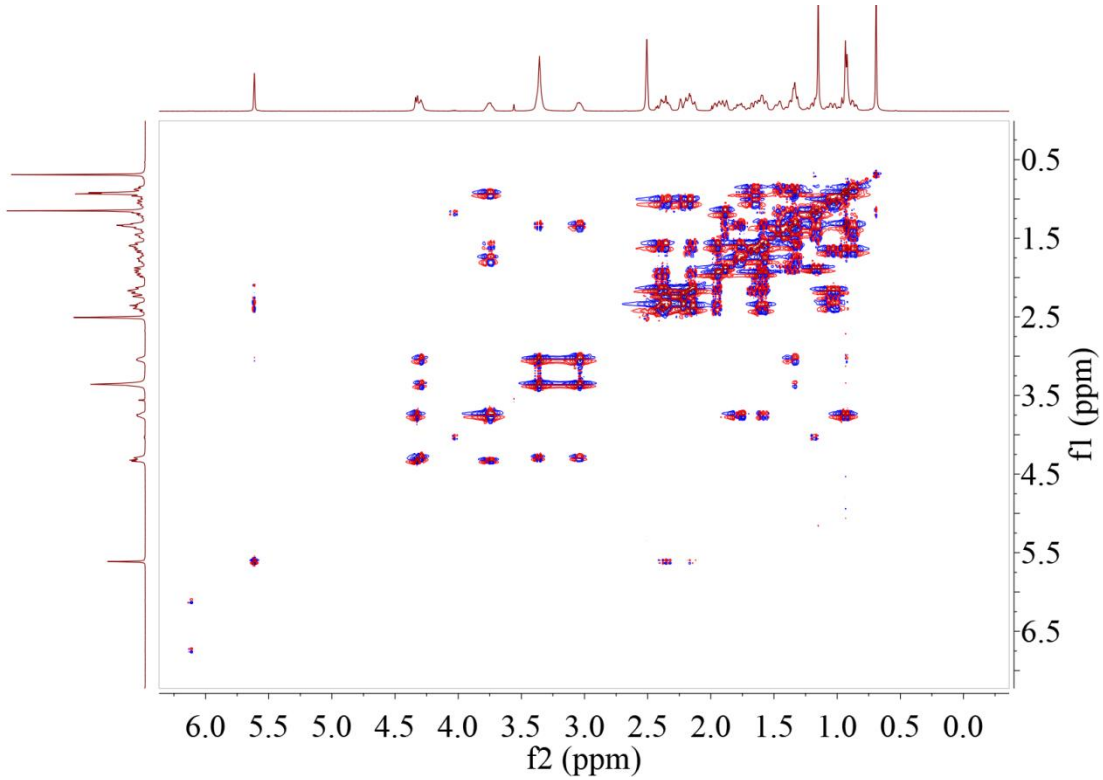

Supplementary Figure 29. ^{1}H-^{1}H COSY spectrum of 15α-hydroxy-bisnoralcohol in DMSO-*d*6 (400 MHz for ^{1}H).

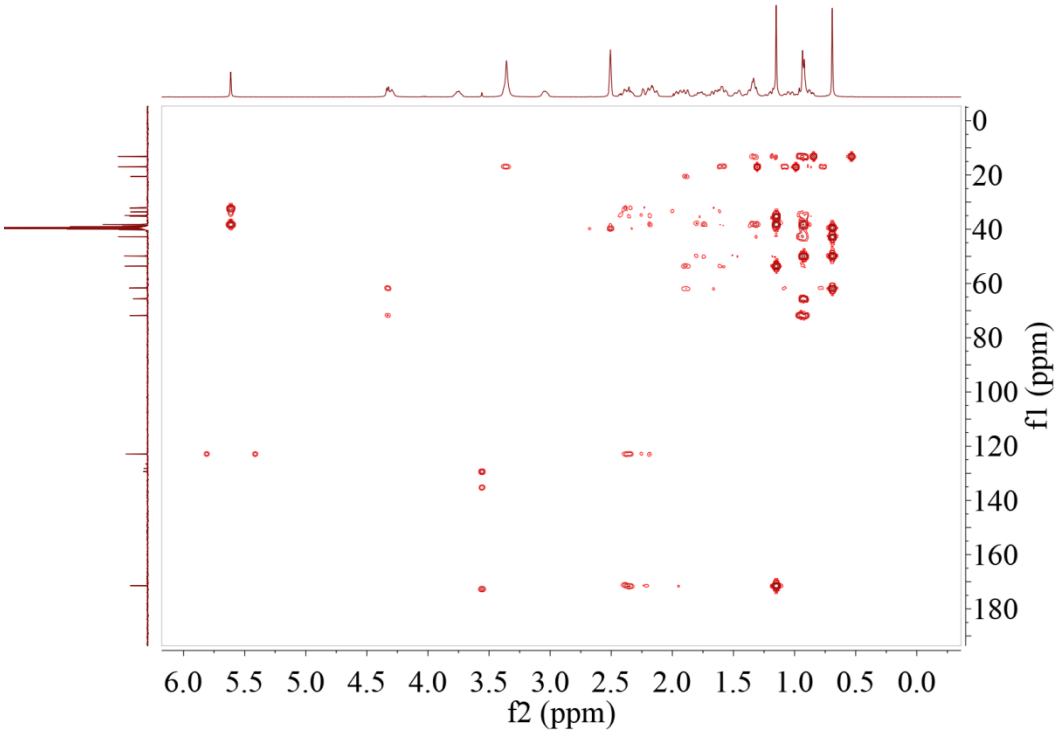

Supplementary Figure 30. HMBC spectrum of 15α-hydroxy-bisnoralcohol in DMSO-*d*6 (400 MHz for ^{1}H, 100 MHz for ^{13}C).

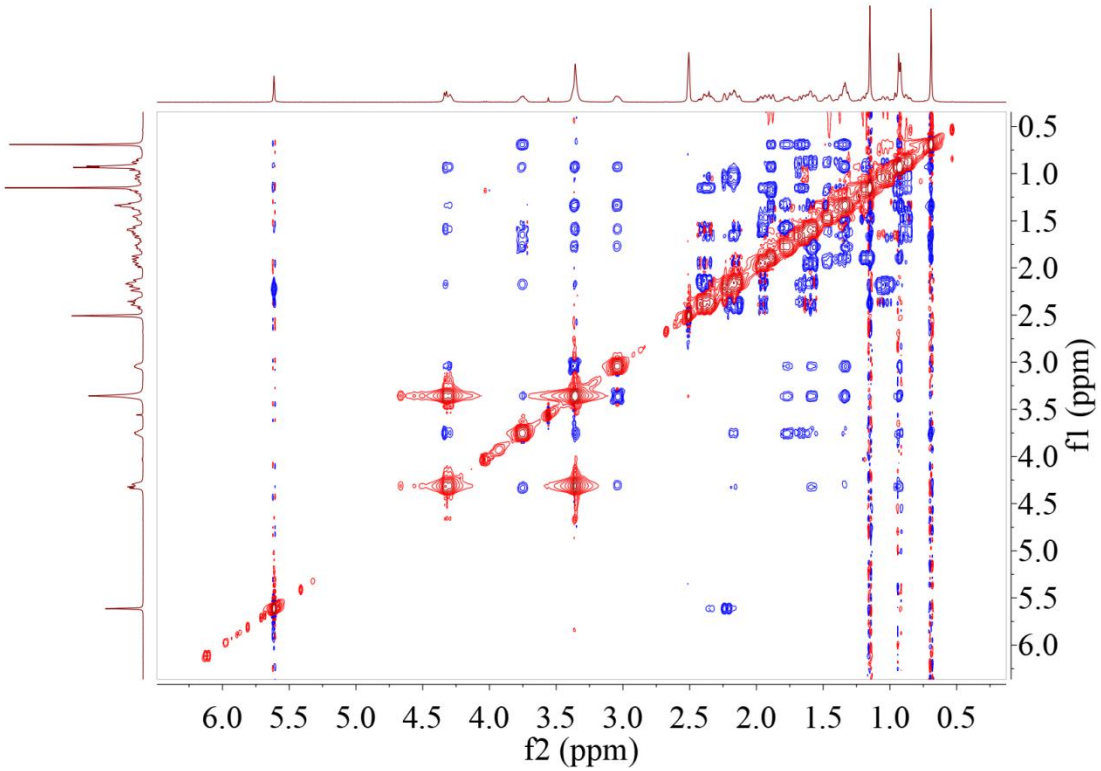

Supplementary Figure 31. NOESY spectrum of 15α-hydroxy-bisnoralcohol in DMSO-*d*6 (400 MHz).

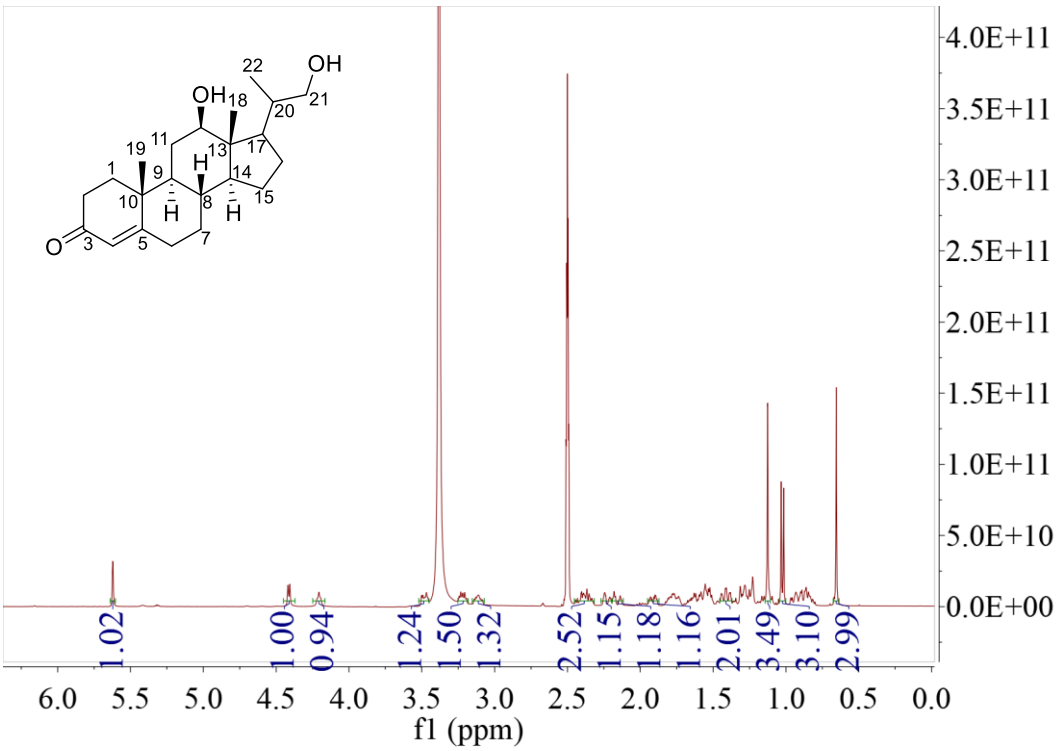

Supplementary Figure 32. ^{1}H NMR spectrum of 12β-hydroxy-bisnoralcohol in DMSO-*d*6 (400 MHz).

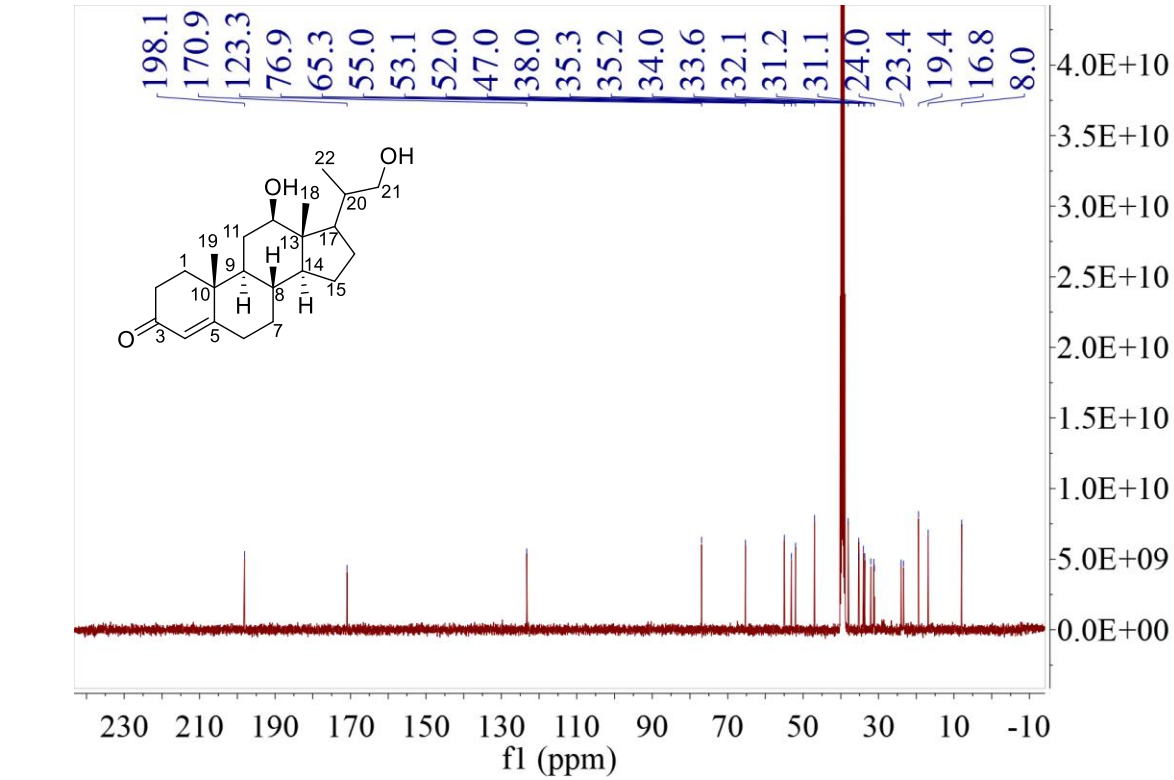

Supplementary Figure 33. ^{13}C NMR spectrum of 12β-hydroxy-bisnoralcohol in DMSO-*d*6 (100 MHz).

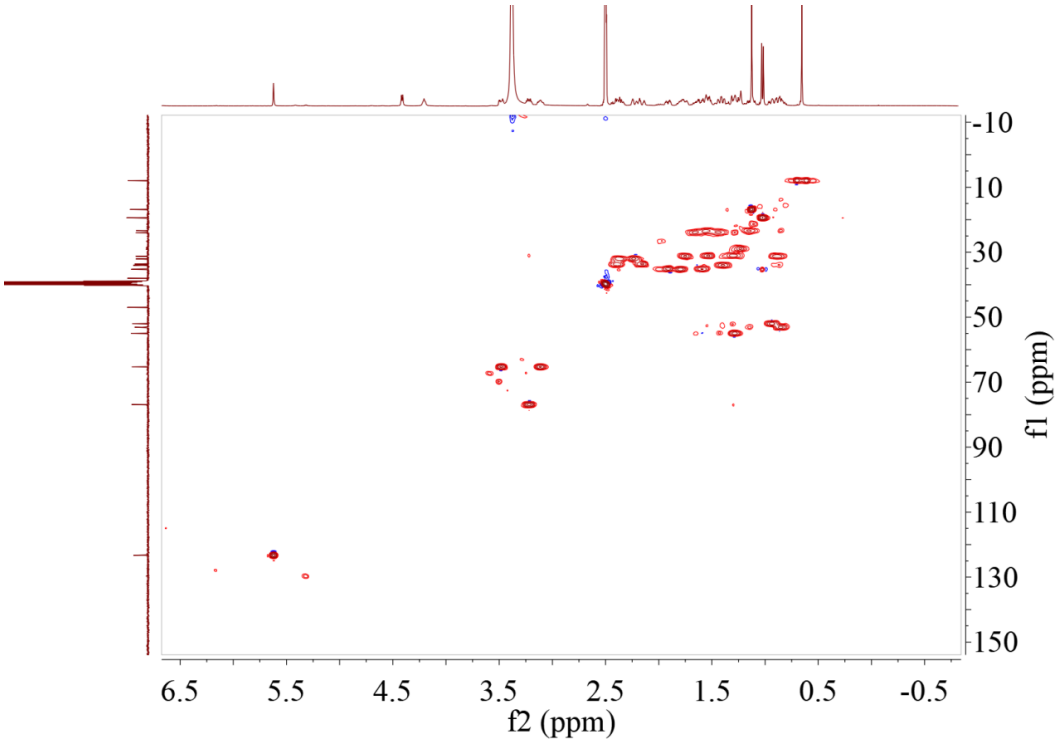

Supplementary Figure 34. HSQC spectrum of 12β-hydroxy-bisnoralcohol in DMSO-*d*6 (400 MHz for ^{1}H, 100 MHz for ^{13}C).

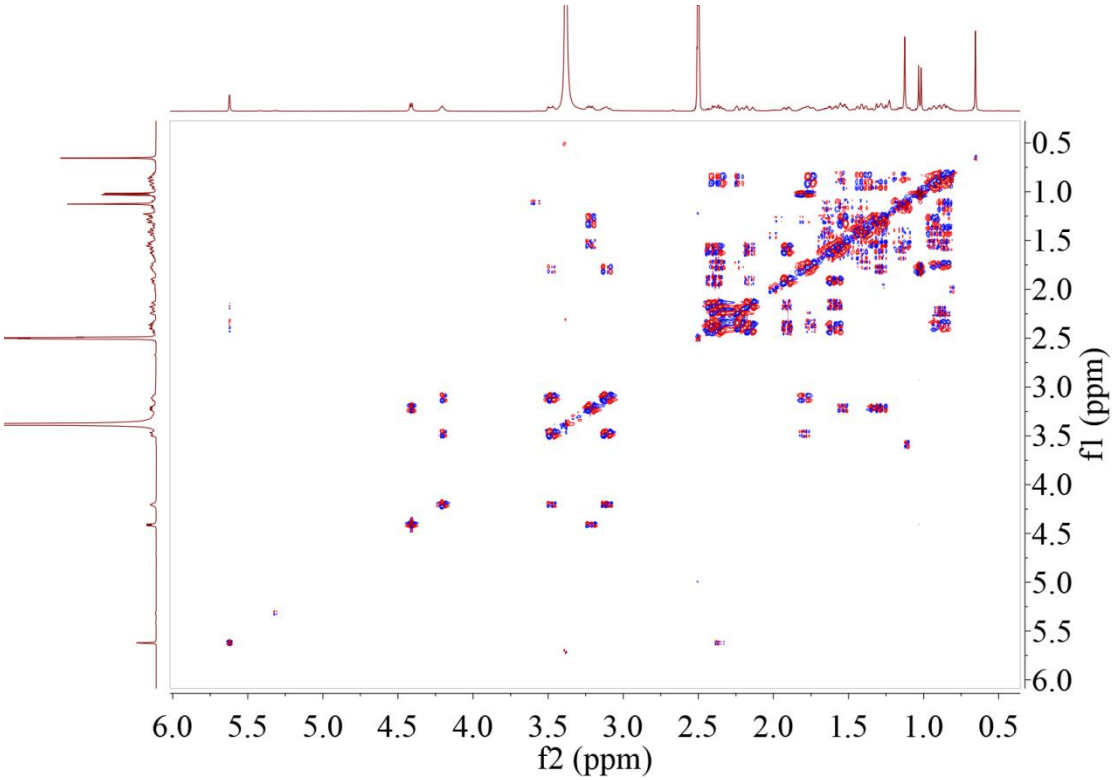

Supplementary Figure 35. ^{1}H-^{1}H COSY spectrum of 12β-hydroxy-bisnoralcohol in DMSO-*d*6 (400 MHz for ^{1}H).

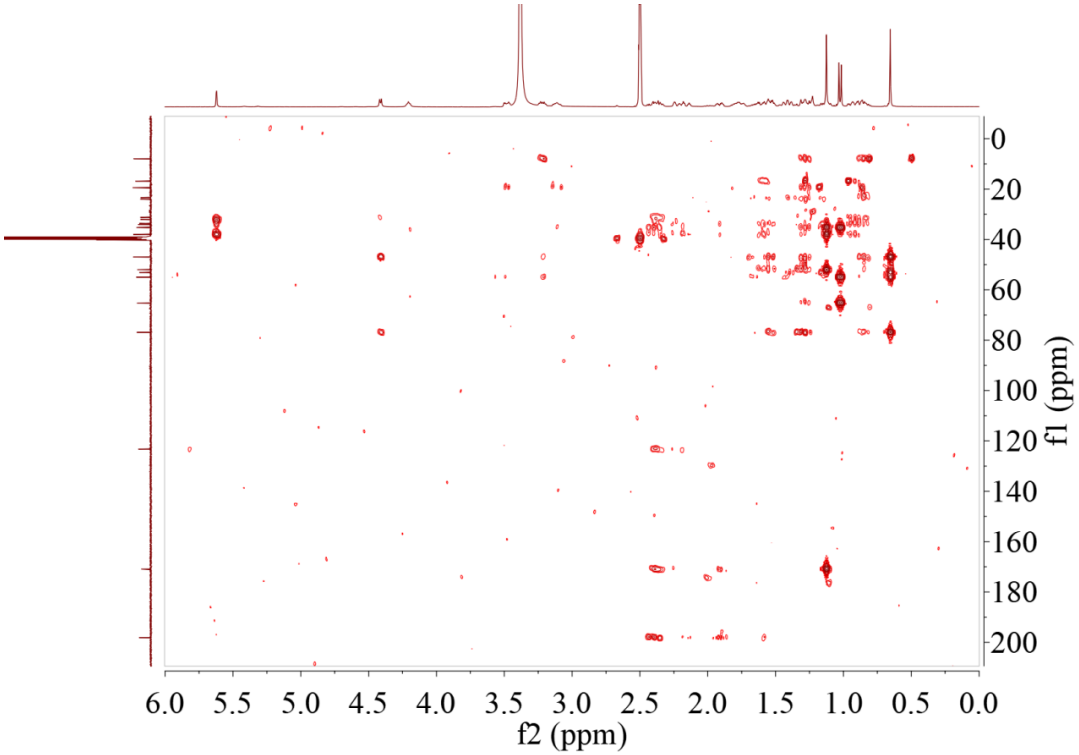

Supplementary Figure 36. HMBC spectrum of 12*β*-hydroxy-bisnoralcohol in DMSO-*d*6 (400 MHz for ^{1}H, 100 MHz for ^{13}C).

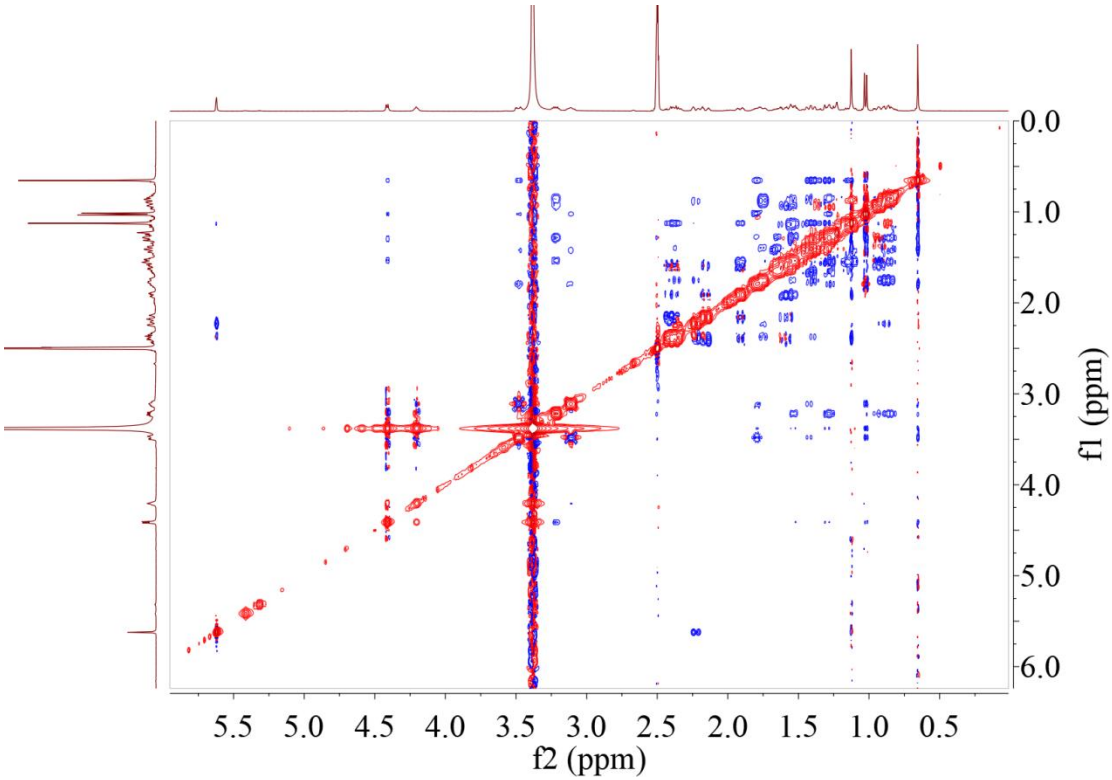

Supplementary Figure 37. NOESY spectrum of 12*β*-hydroxy-bisnoralcohol in DMSO-*d*6 (400 MHz).

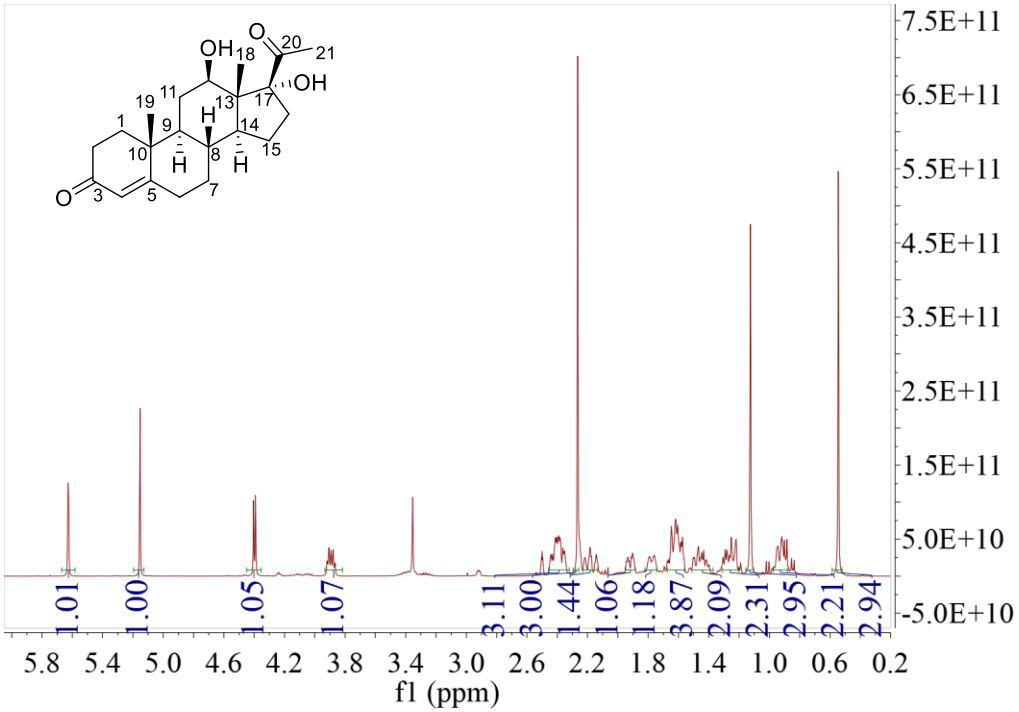

Supplementary Figure 38. [1]H NMR spectrum of 12*β*, 17*α*-dihydroxy-progesterone in DMSO-*d*6 (400 MHz).

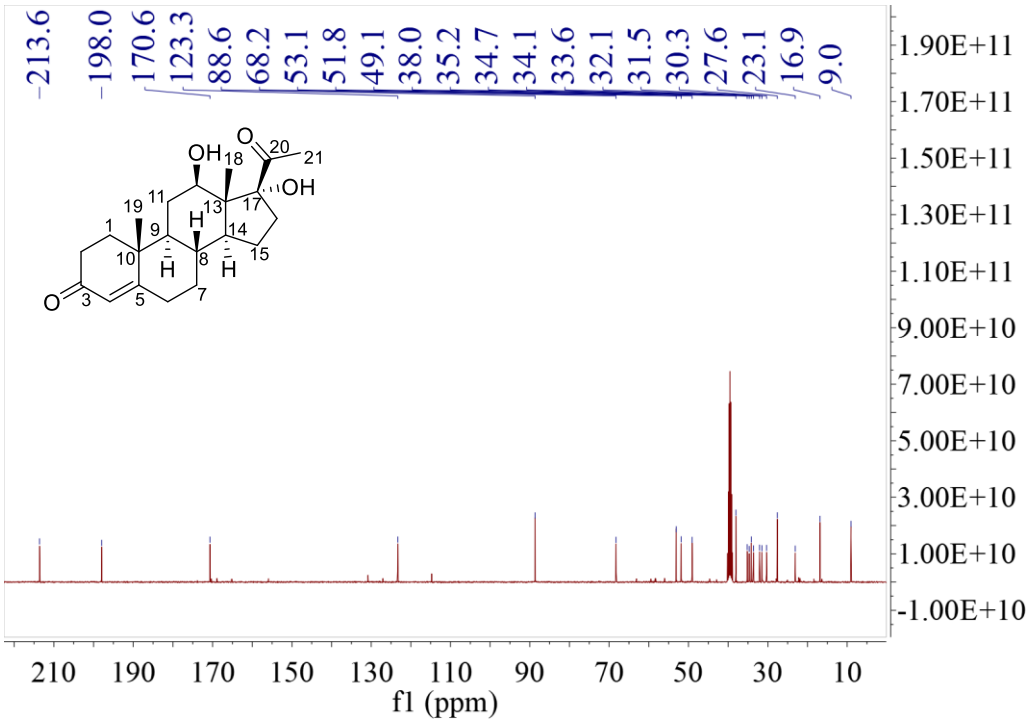

Supplementary Figure 39. [13]C NMR spectrum of 12*β*, 17*α*-dihydroxy-progesterone in DMSO-*d*6 (100 MHz).

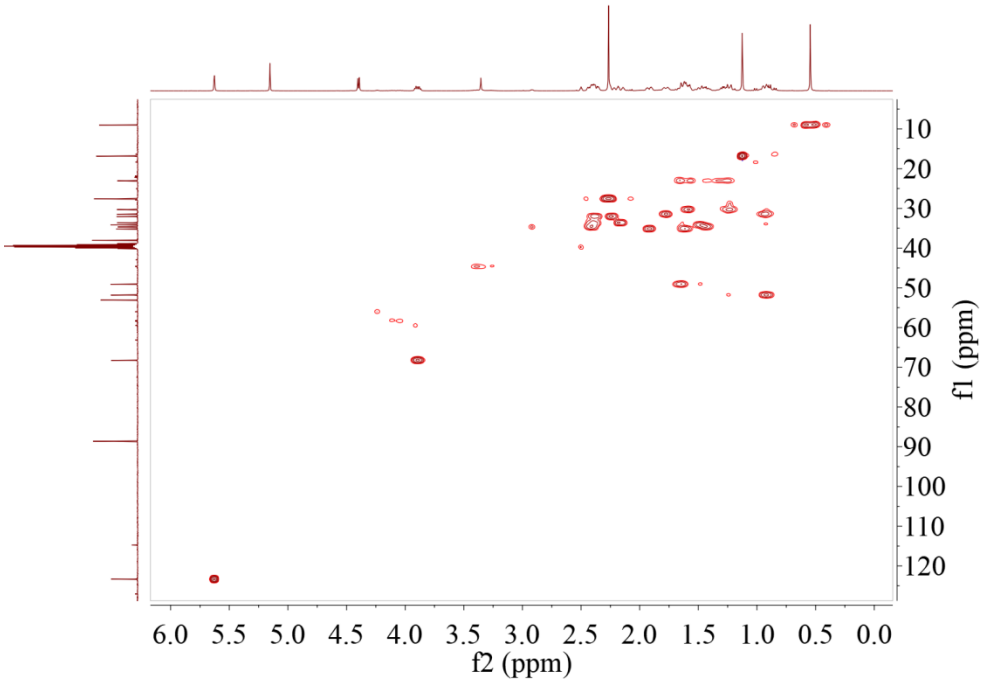

Supplementary Figure 40. HSQC spectrum of 12β, 17α-dihydroxy-progesterone in DMSO-*d*6 (400 MHz for ^{1}H, 100 MHz for ^{13}C).

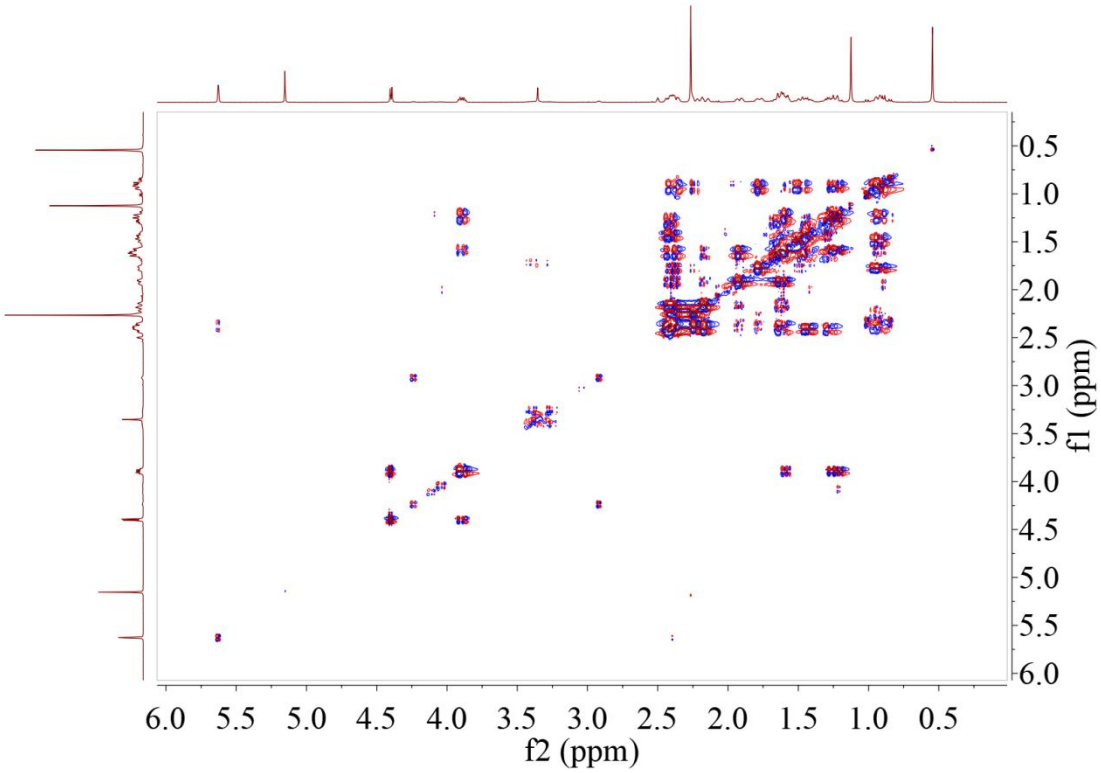

Supplementary Figure 41. ^{1}H-^{1}H COSY spectrum of 12β, 17α-dihydroxy-progesterone in DMSO-*d*6 (400 MHz for ^{1}H).

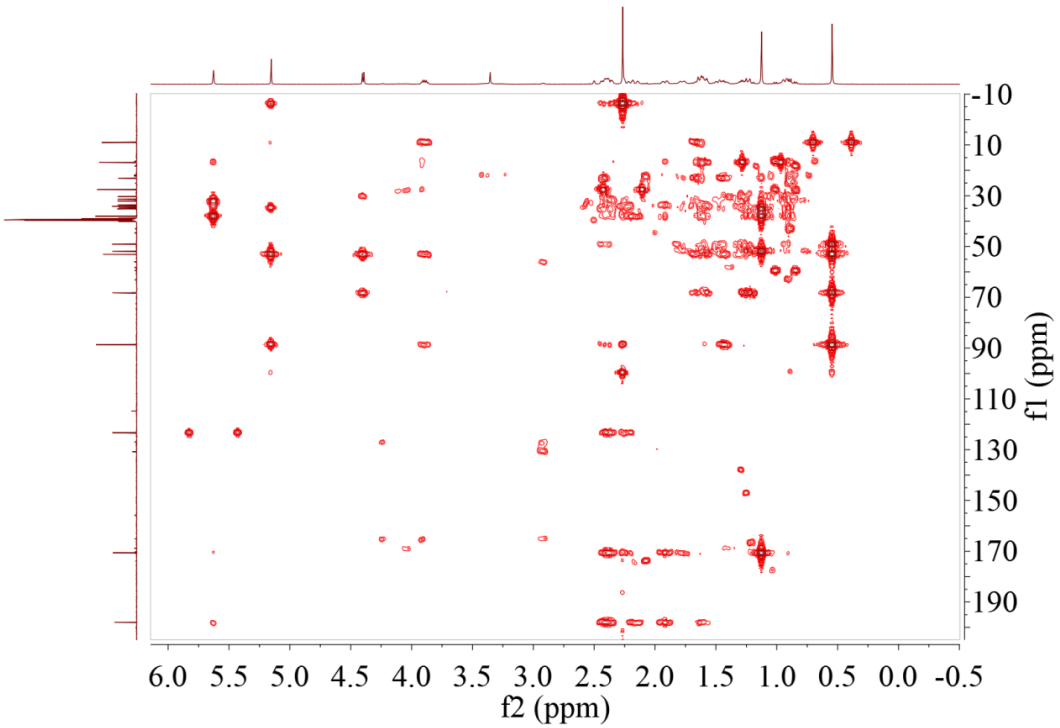

Supplementary Figure 42. HMBC spectrum of 12β, 17α-dihydroxy-progesterone in DMSO-*d*6 (400 MHz for ^{1}H, 100 MHz for ^{13}C).

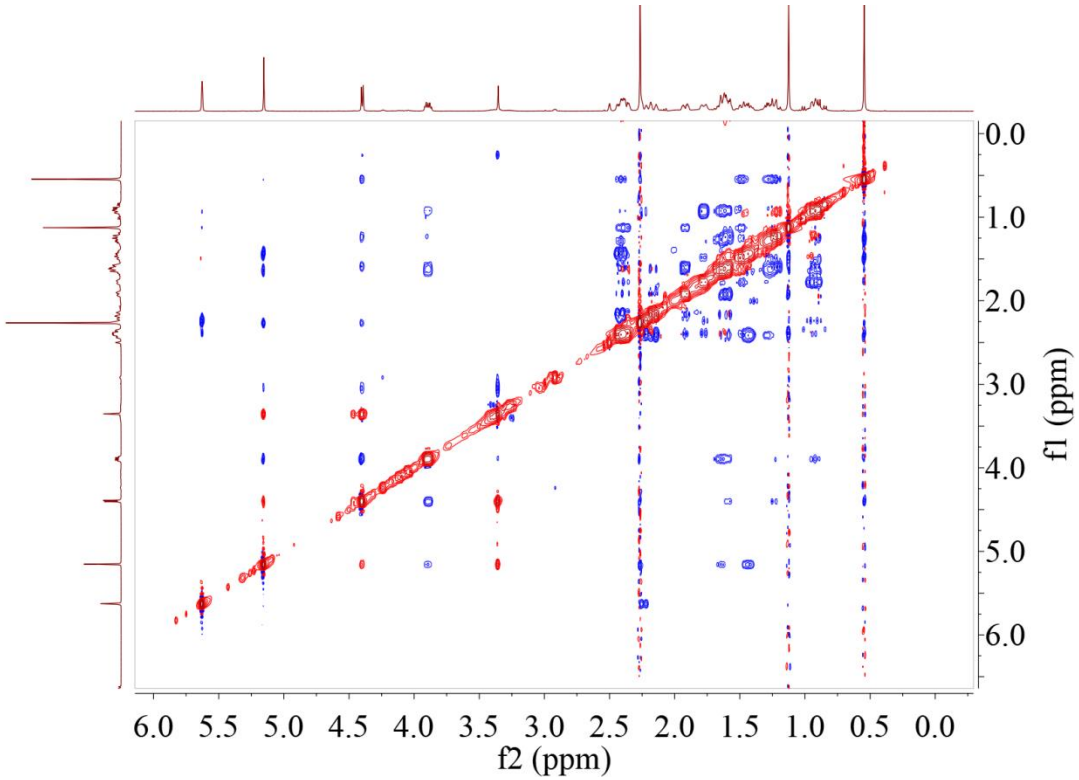

Supplementary Figure 43. NOESY spectrum of 12β, 17α-dihydroxy-progesterone in DMSO-*d*6 (400 MHz).

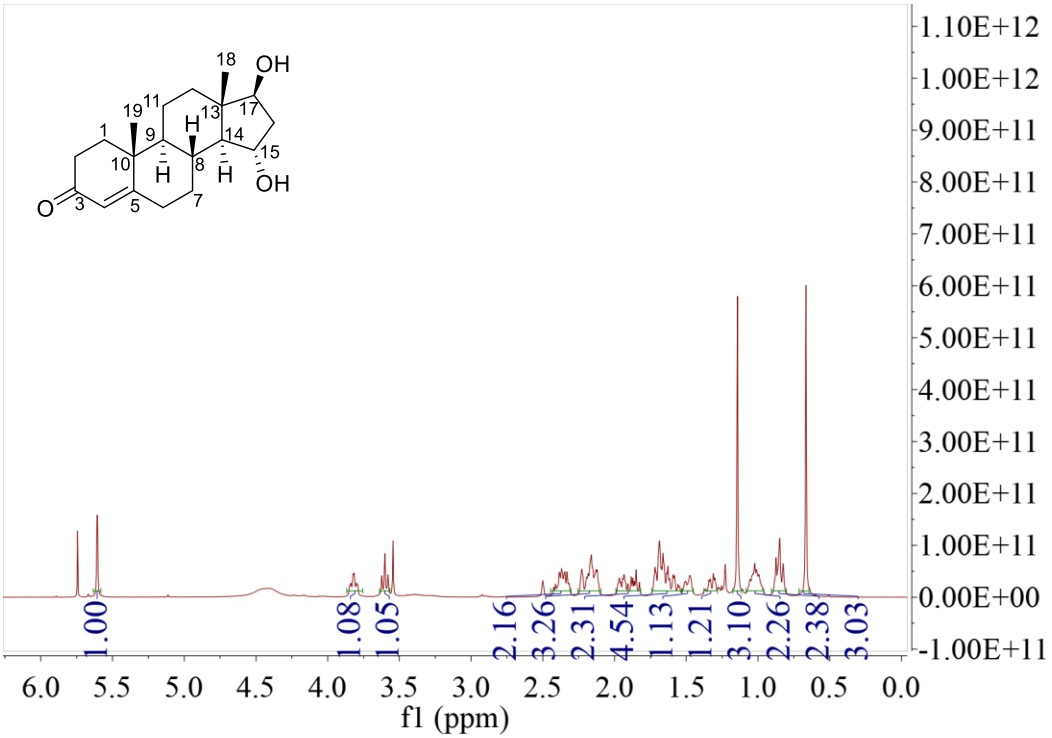

Supplementary Figure 44. [1]H NMR spectrum of 15*α*-hydroxy-testosterone in DMSO-*d*6 (400 MHz).

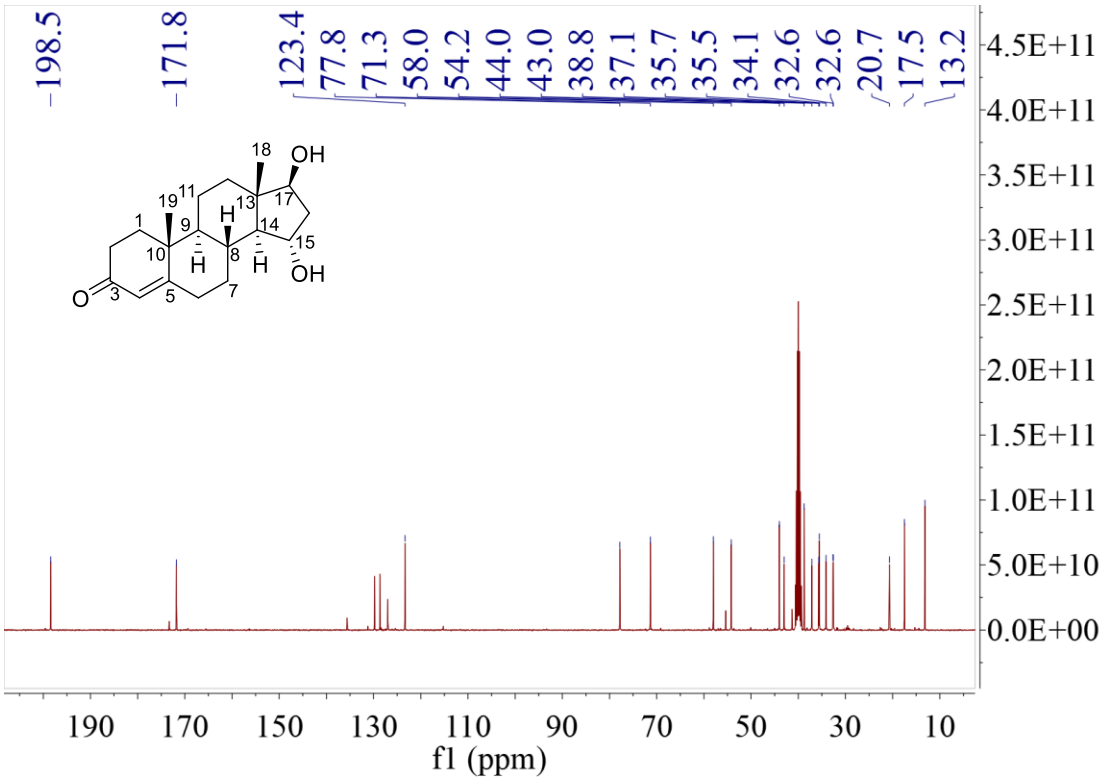

Supplementary Figure 45. [13]C NMR spectrum of 15*α*-hydroxy-testosterone in DMSO-*d*6 (100 MHz).

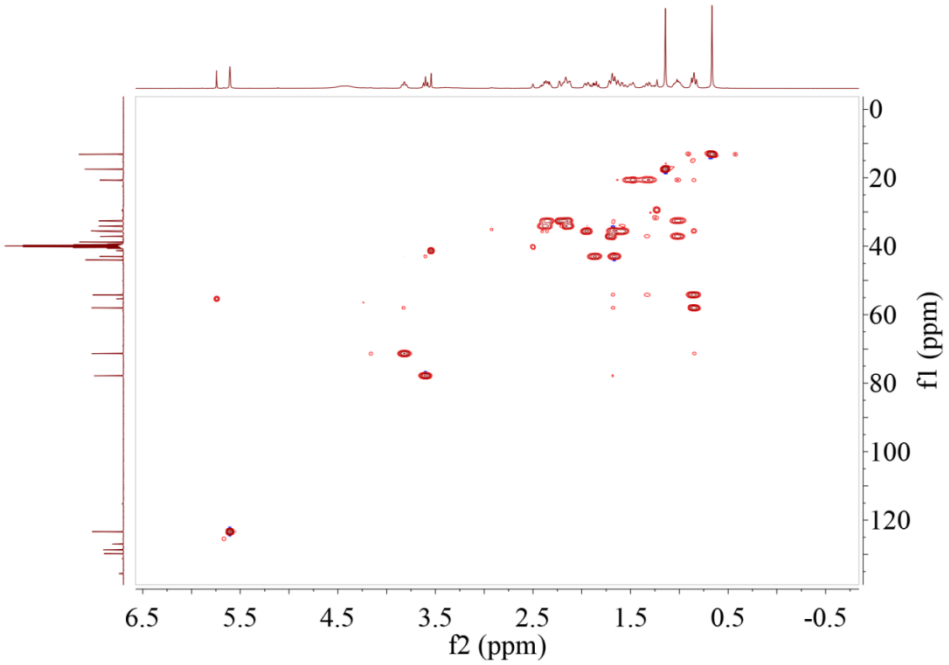

Supplementary Figure 46. HSQC spectrum of 15α-hydroxy-testosterone in DMSO-*d*6 (400 MHz for ^{1}H, 100 MHz for ^{13}C).

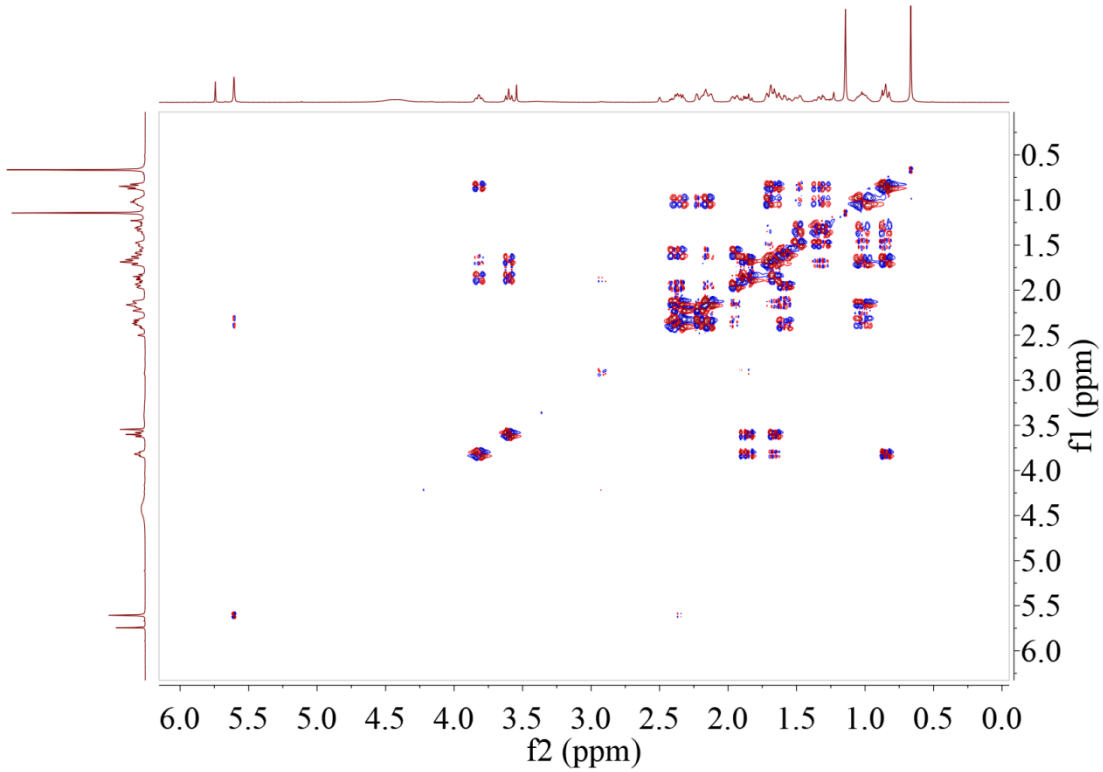

Supplementary Figure 47. ^{1}H-^{1}H COSY spectrum of 15α-hydroxy-testosterone in DMSO-*d*6 (400 MHz for ^{1}H).

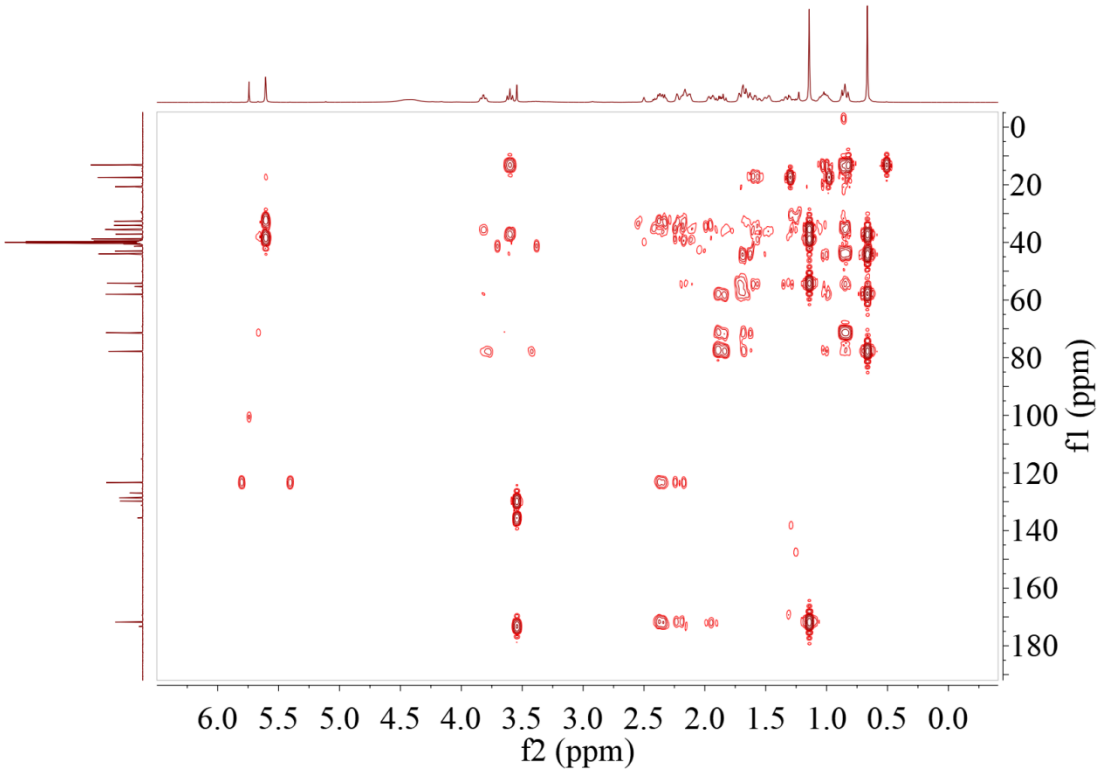

Supplementary Figure 48. HMBC spectrum of 15α-hydroxy-testosterone in DMSO-*d*6 (400 MHz for ^{1}H, 100 MHz for ^{13}C).

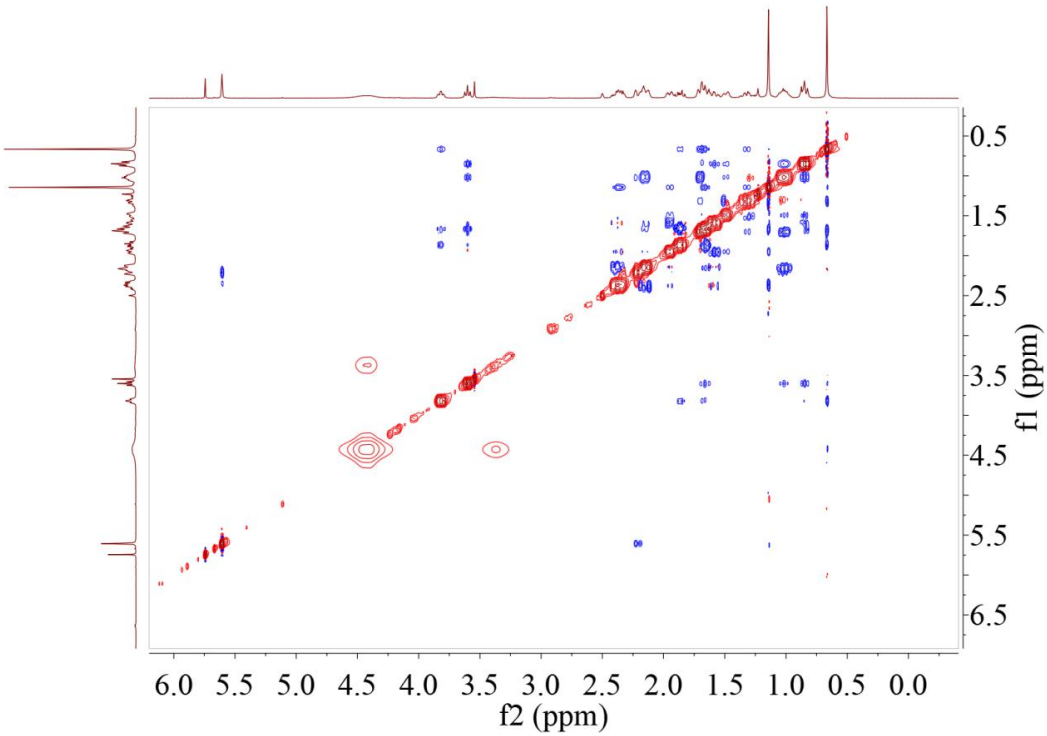

Supplementary Figure 49. NOESY spectrum of 15α-hydroxy-testosterone in DMSO-*d*6 (400 MHz).

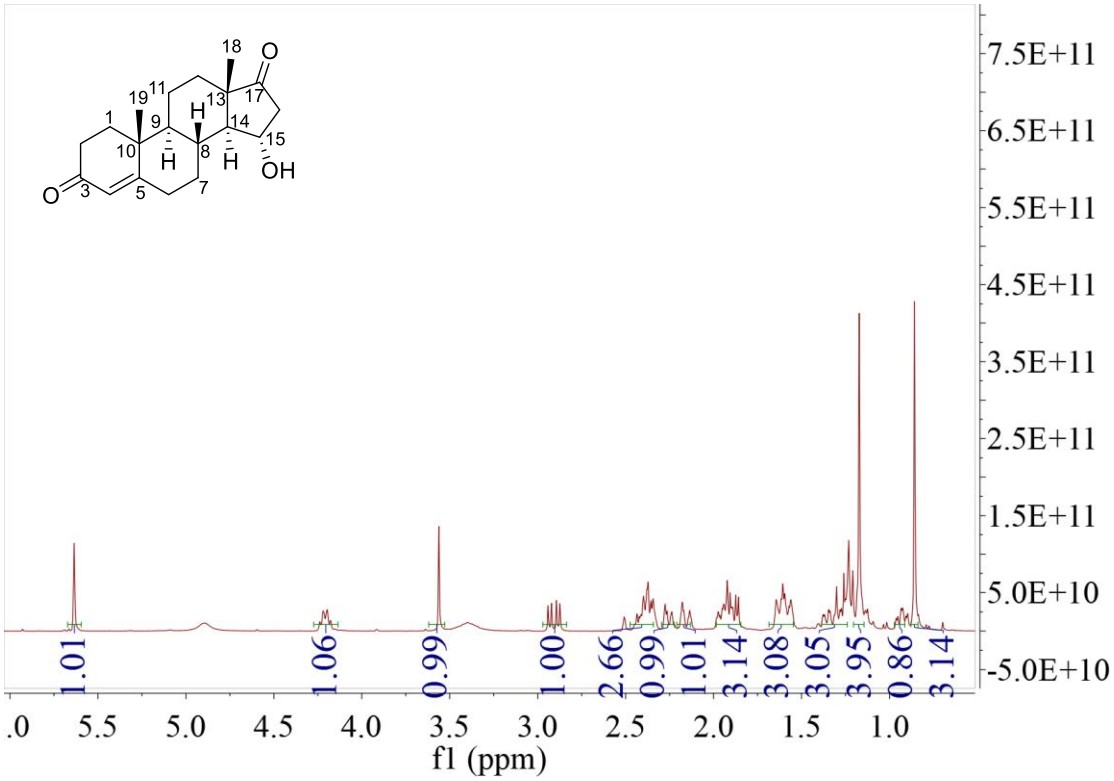

Supplementary Figure 50. [1]H NMR spectrum of 15*α*-hydroxy-androstenedione in DMSO-*d*6 (400 MHz).

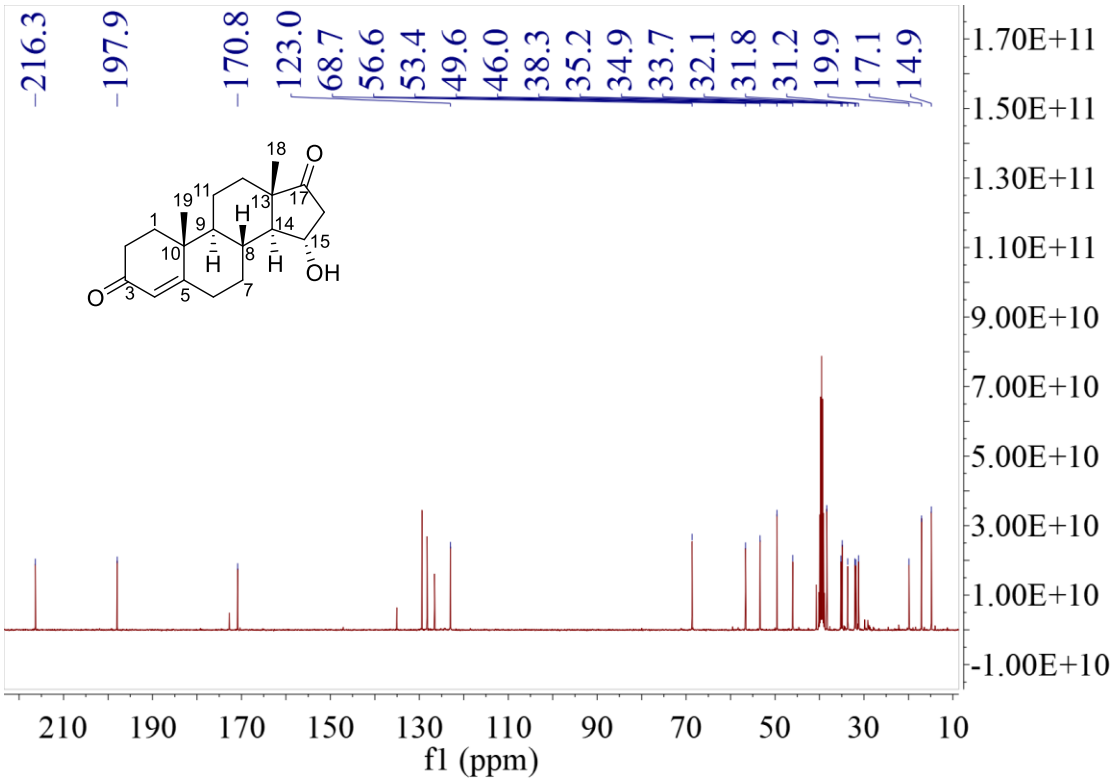

Supplementary Figure 51. [13]C NMR spectrum of 15*α*-hydroxy-androstenedione in DMSO-*d*6 (100 MHz).

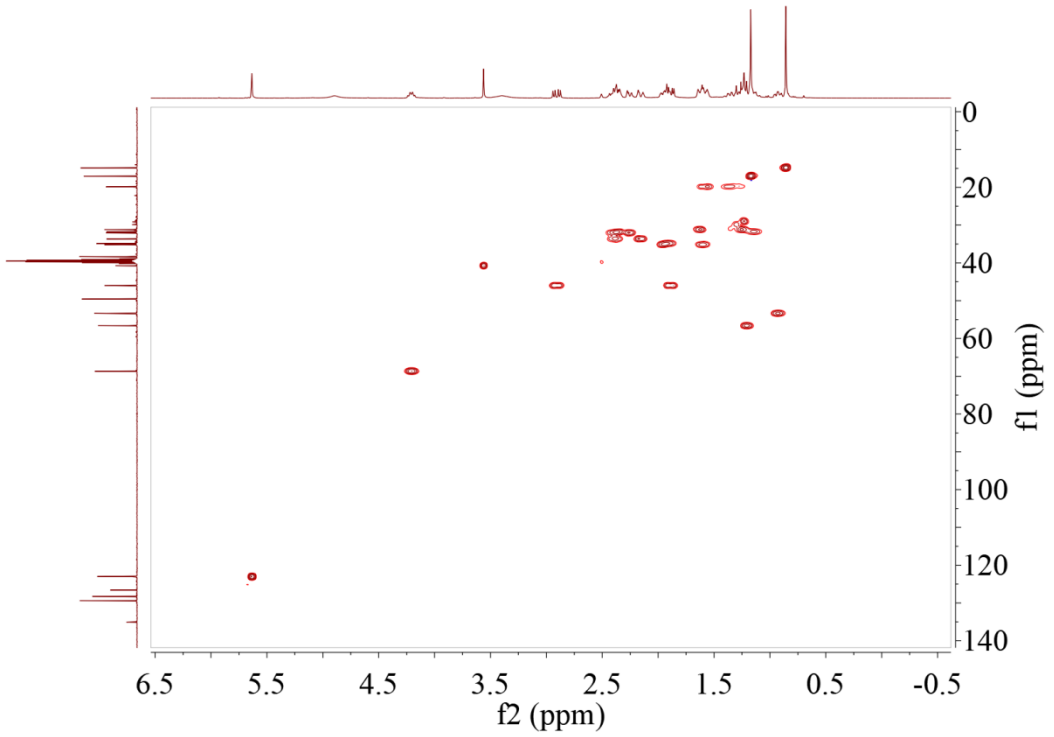

Supplementary Figure 52. HSQC spectrum of 15α-hydroxy-androstenedione in DMSO-*d*6 (400 MHz for ^{1}H, 100 MHz for ^{13}C).

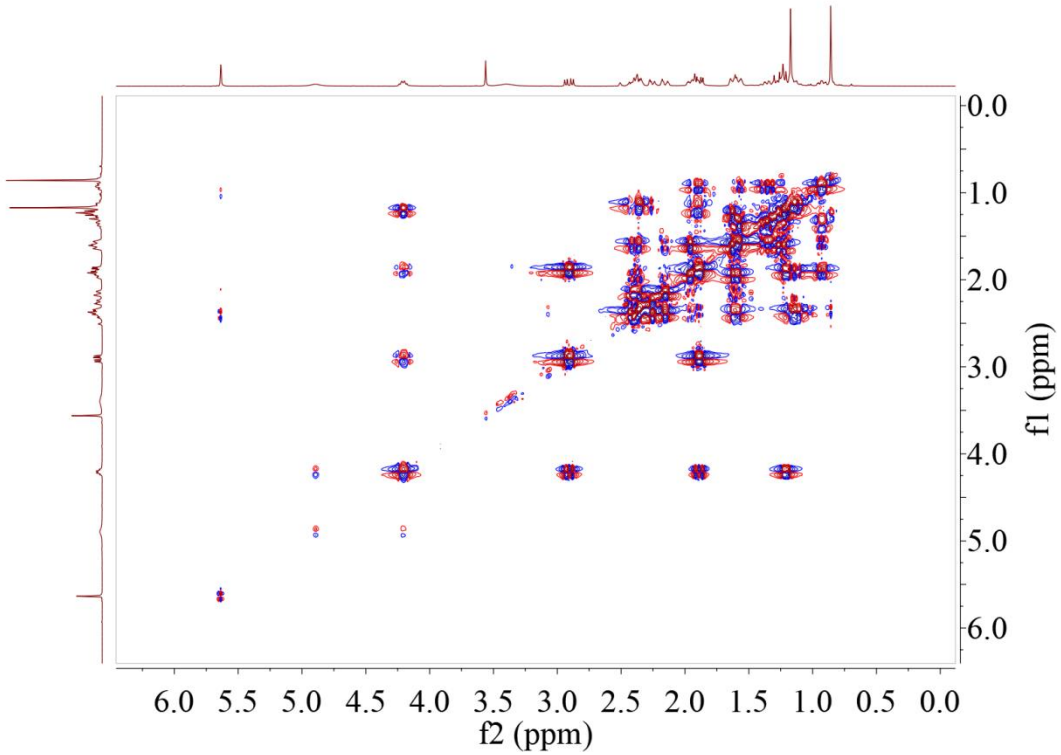

Supplementary Figure 53. ^{1}H-^{1}H COSY spectrum of 15α-hydroxy-androstenedione in DMSO-*d*6 (400 MHz for ^{1}H).

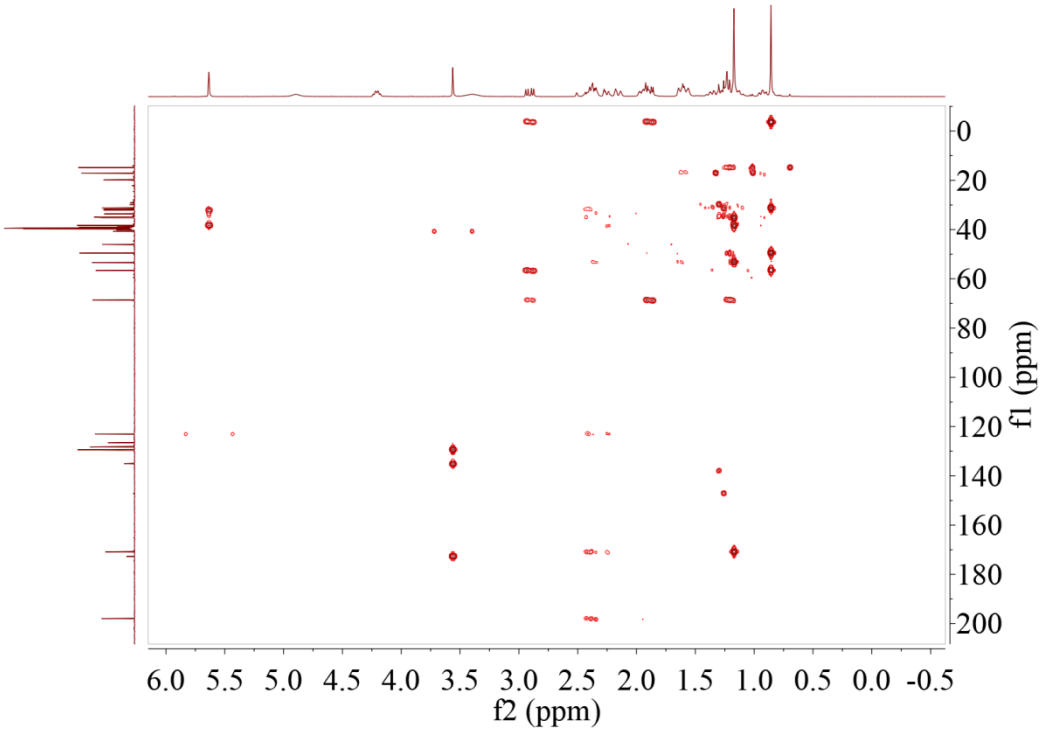

Supplementary Figure 54. HMBC spectrum of 15*α*-hydroxy-androstenedione in DMSO-*d*6 (400 MHz for ^{1}H, 100 MHz for ^{13}C).

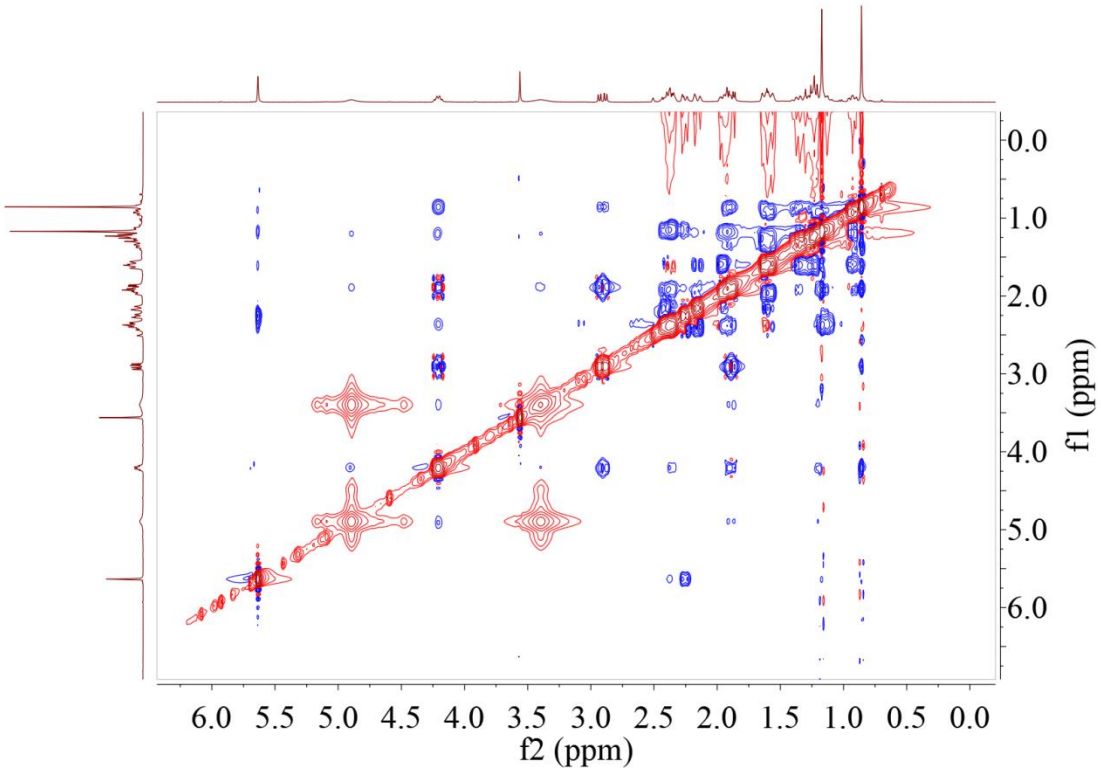

Supplementary Figure 55. NOESY spectrum of 15*α*-hydroxy-androstenedione in DMSO-*d*6 (400 MHz).

Supplementary Figures for HR-EMIMS

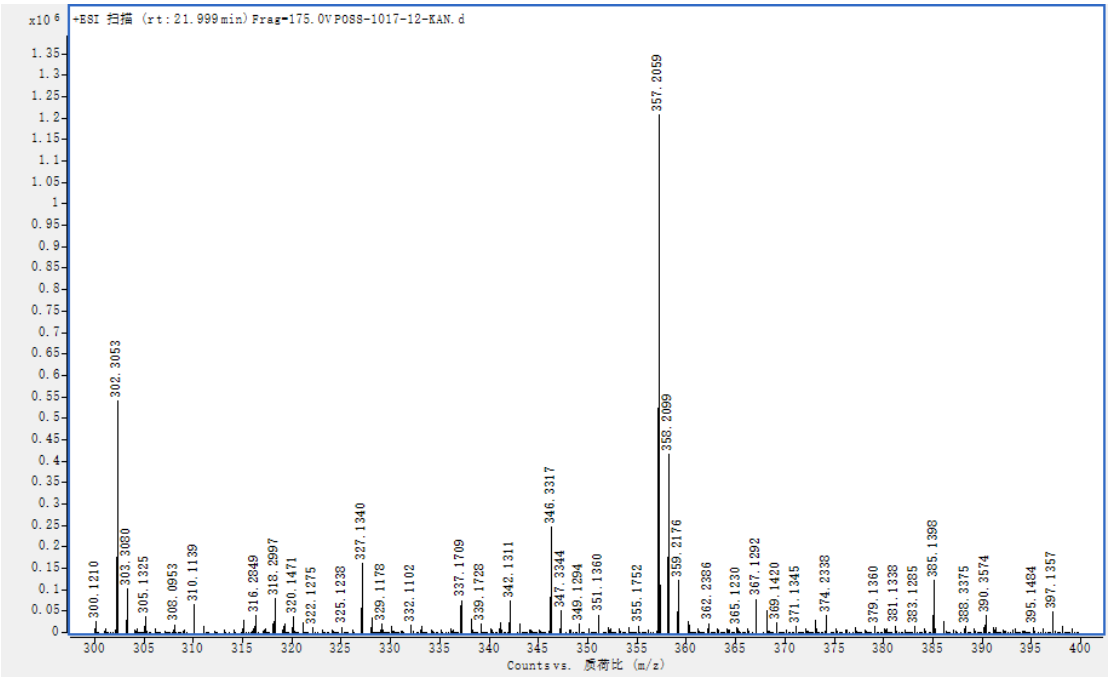

Supplementary Figure 56. HR-ESIMS data of 12β-hydroxy-canrenone.

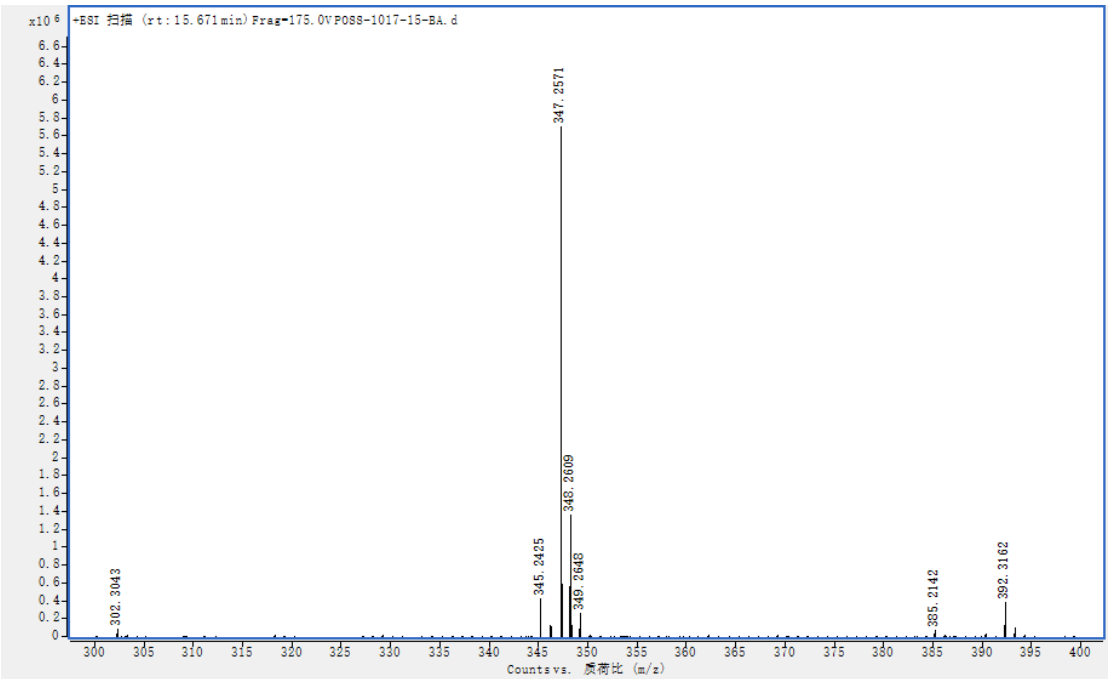

Supplementary Figure 57. HR-ESIMS data of 15α-hydroxy-bisnoralcohol.

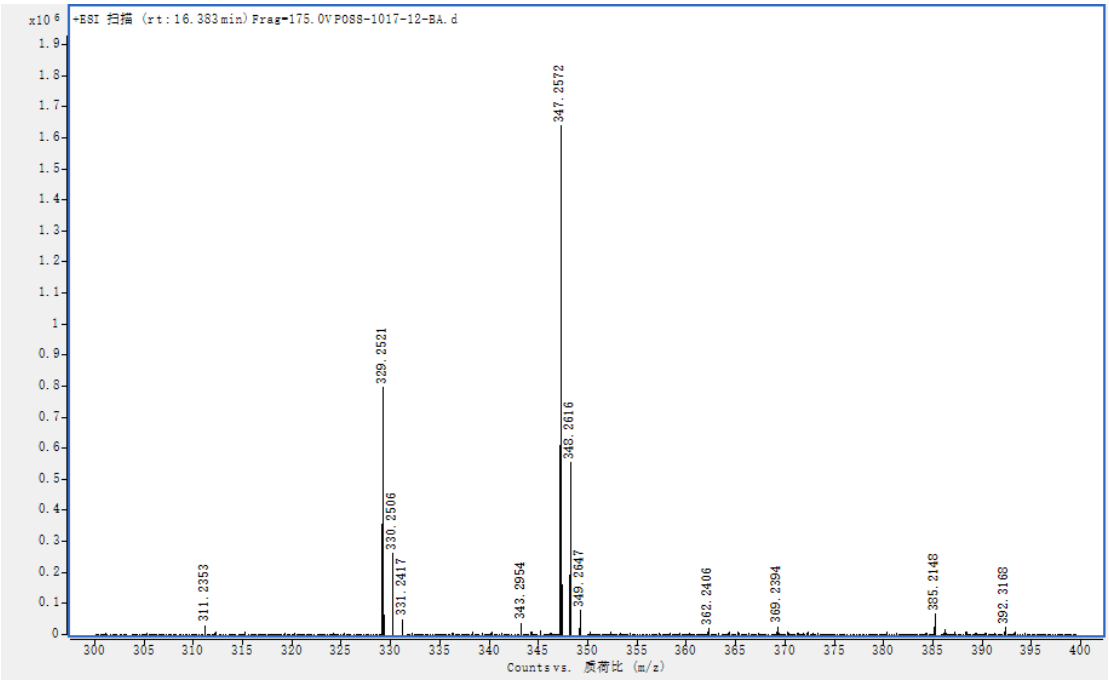

Supplementary Figure 58. HR-ESIMS data of 12*β*-hydroxy-bisnoralcohol.

Supplementary References

1 Wang, L. *et al.* A fungal P450 enzyme from *Fusarium graminearum* with unique 12*β*-steroid hydroxylation activity. *Appl. Environ. Microbiol.* **89**, e01963-01922 (2023).

2 Vico, P., Cauet, G., Rose, K., Lathe, R. & Degryse, E. Dehydroepiandrosterone (DHEA) metabolism in *Saccharomyces cerevisiae* expressing mammalian steroid hydroxylase CYP7B: Ayr1p and Fox2p display 17*β*-hydroxysteroid dehydrogenase activity. *Yeast* **19**, 873-886, (2002).